# The Mechanics of Neutrophils: Synthetic Modeling of Three Experiments

Marc Herant, William A. Marganski, and Micah Dembo
Biomedical Engineering Department, Boston University, Boston, Massachusetts 02215

ABSTRACT Much experimental data exist on the mechanical properties of neutrophils, but so far, they have mostly been approached within the framework of liquid droplet models. This has two main drawbacks: 1), It treats the cytoplasm as a single phase when in reality, it is a composite of cytosol and cytoskeleton; and 2), It does not address the problem of active neutrophil deformation and force generation. To fill these lacunae, we develop here a comprehensive continuum-mechanical paradigm of the neutrophil that includes proper treatment of the membrane, cytosol, and cytoskeleton components. We further introduce two models of active force production: a cytoskeletal swelling force and a polymerization force. Armed with these tools, we present computer simulations of three classic experiments: the passive aspiration of a neutrophil into a micropipette, the active extension of a pseudopod by a neutrophil exposed to a local stimulus, and the crawling of a neutrophil inside a micropipette toward a chemoattractant against a varying counterpressure. Principal results include: 1), Membrane cortical tension is a global property of the neutrophil that is affected by local area-increasing shape changes. We argue that there exists an area dilation viscosity caused by the work of unfurling membrane-storing wrinkles and that this viscosity is responsible for much of the regulation of neutrophil deformation. 2), If there is no swelling force of the cytoskeleton, then it must be endowed with a strong cohesive elasticity to prevent phase separation from the cytosol during vigorous suction into a capillary tube. 3), We find that both swelling and polymerization force models are able to provide a unifying fit to the experimental data for the three experiments. However, force production required in the polymerization model is beyond what is expected from a simple short-range Brownian ratchet model. 4), It appears that, in the crawling of neutrophils or other amoeboid cells inside a micropipette, measurement of velocity versus counterpressure curves could provide a determination of whether cytoskeleton-to-cytoskeleton interactions (such as swelling) or cytoskeleton-to-membrane interactions (such as polymerization force) are predominantly responsible for active protrusion.

## INTRODUCTION

The mechanical properties of the neutrophil are closely related to its function as the primary foot soldier of the immune system. As such, it has been a favorite subject of experiments aimed at characterizing its ability to change shape and generate forces as dictated by circumstance. This is why, over the last decades, an impressive amount of qualitative and quantitative data have been collected on the mechanical behavior of neutrophils at the macroscopic scale accessible to visible light microscopy. At the same time, investigations at the microscopic level defined by molecular biology techniques have elucidated a number of biochemical pathways. However, despite these efforts, the phenomenology of neutrophil mechanics has lagged, insofar as it has been principally restricted to extensions of liquid droplet models (e.g., see Yeung and Evans, 1989; Drury and Dembo, 2001). This approach has the drawback that it ignores the dual nature of the cytoplasm with its cytosolic and cytoskeletal phases. It also is clearly insufficient to address problems of active motion.

The goal of this article is to begin to bridge the gap between microscopy and biochemistry with a mesoscopic paradigm of neutrophil mechanics applicable to a wide variety of experimental conditions. Within the framework of continuum mechanics, we will propose and discuss simple models, and carry out a numerical analysis of their consequences in the setting of various experiments. Our objective is not to obtain perfect agreement with experimental data, nor is it to provide a detailed connection with biochemical processes. Rather, we are interested in developing synthetic models that can serve as an intuitively accessible but self-consistent context in which the profusion of experimental evidence can be coordinated, and new experiments devised. Depending on taste and personal bias, these models are to be a foundation or a ''straw man'' that can be further expanded, revised, or contested. Regardless, their principal merit lies in their ability to organize ideas on neutrophil behavior.

In vivo, it is felt that the neutrophil exists in two basic states. In the quiescent or passive state, the neutrophil simply flows with the blood circulation deforming passively with minimal disturbance to its environment. In contrast, the activated state represents a response to inflammatory stimulus: in this incarnation the neutrophil is capable of actively developing forces that lead to adhesion and deformation. Of all the experiments devised to study the two faces of the neutrophil, a few stand out as particularly instructive because they capture some essential aspect of neutrophil mechanics, and because they can be built on to address more complex phenomena:

1. The aspiration of a passive neutrophil into a micropipette provides powerful constraints on mechanical properties

*Submitted August 23, 2002, and accepted for publication January 13, 2003.*

Address reprint requests to Micah Dembo, 44 Cummington St., Boston University, Boston, MA 02215. Tel.: 617-353-1671; Fax: 617-353-6766; E-mail: mxd@bu.edu.



0006-3495/03/05/3389/25 $2.00

on the basis of rate of entry versus time for various aspiration pressures and pipette radii.
2. The local stimulation of a neutrophil with fMLP with subsequent pseudopod formation represents the most elementary active shape-changing process that can be conceived.
3. The motion of an activated neutrophil in a micropipette toward a chemoattractant against an opposing pressure provides the simplest quantitative measurement of the production of active force.

This article is about offering a synthesis of these three experiments from the point of view of the laws of continuum mechanics. In this endeavor, we shall introduce two different models that have been proposed in the past to explain cellular force generation and shape stabilization. One postulates a general spontaneous repulsive (expansive) force of the cytoskeleton and will be called the swelling model. The other assumes directed force generation at the membrane through polymerization and will be called the polymerization force model. We will present numerical simulations that exhibit the qualitative behavior of each model and that allow one to determine the quantitative parameters required to fit the observed data.

It is worth noting that although it may not be always directly apparent to the reader, almost all the qualitative features and quantitative parameters that figure in our models are deeply interconnected. To keep things tractable, it has been necessary to present experiments sequentially and to order the discussion of the impact of various physical parameters in a succession of individual items (e.g., elasticity, viscosity, swelling, etc.). However, this neat organization obscures the entanglement between all the factors determining neutrophil behavior, which basically makes it impossible to change one thing in a model without changing everything in that model. As a consequence, our models have de facto undergone a stringent portability test by which parameters determined by a particular experiment are validated by other experiments.

## CONTINUUM MECHANICS AND REACTIVE INTERPENETRATING FLOWS

### Basic concepts

From a mechanical standpoint, neutrophils are made up of three main constituent components: a relatively impermeable membrane (in the sense that the cell maintains a constant volume), an aqueous solvent phase, and a cytoskeletal network phase. It is also clear that the solvent phase is in large part a passive player, as it cannot transmit significant stresses other than through a banal pressure field. Although it is a medium through which all manner of chemical signals are diffusing, by itself the solvent is a bystander that flows through the network as required by volume conservation: swelling in one area of the cell draws water from other parts, while contraction does the opposite.

The principal actors of neutrophil mechanics (and for that matter, many amoeboid cells) are therefore the membrane and the cytoskeleton. The membrane contributes primarily through the surface tension whose meaning and form will be discussed in greater detail (see Membrane Surface Tension) and through boundary conditions imposed by contact surfaces. On the other hand, the mechanical properties of the network are the predominant source of richness of neutrophil behavior and, at the same time, the predominant source of controversy in this area of study. Despite this complexity, a few reasonable general statements can be made. First, the cytoskeleton is able to offer passive resistance to changes in shape; this means that the cytoskeleton is endowed with elastic and/or viscous properties that oppose deformation. Second, the stimulated cytoskeleton is able to produce active forces that result in spontaneous movement, and thus changes of shape. Several classes of forces can be envisioned to be responsible for this: isotropic network-to-network repulsive interactions leading to a natural swelling tendency of the cytoskeleton; directional polymerization forces involving Brownian ratchets; more general network-to-membrane repulsive potentials; directional molecular motors; etc. Fortunately, the general framework of continuum mechanics is sufficiently broad to allow the inclusion of all those alternatives through modification of the momentum equations.

Finally, it is possible to argue that organelles represent a fourth mechanical constituent of the neutrophil. Small organelles such as mitochondria can probably be subsumed into the bulk properties of the cytoplasm through coarse-graining. However, the nucleus occupies ~20% of the cell volume (Schmid-Schönbein et al., 1980) and it has been argued by some to be a mechanically important entity (Kan et al., 1999). In the neutrophil, the nucleus is made up of three to four segmented lobules tethered together by flexible neck regions like pearls on a string (e.g., see Sanchez and Wangh, 1999; Campbell et al., 1995). This likely is an adaptation to the demands of passage through narrow capillary beds and diapedesis into tissues, the implication being that the nucleus has evolved to be as mechanically unobtrusive as possible. In the interest of simplicity, we therefore neglect to include a separate compartment for the nucleus in our models. Some weak support for this approach is provided by the fact that we get an adequate fit to the data that we are trying to explain.

### Evolution equations

The Reactive Interpenetrating Flow formalism has previously been described in Dembo and Harlow (1986), Dembo (1994a), and He and Dembo (1997). We will therefore limit ourselves to a brief overview. In all that follows, the subscript $s$ denotes solvent-related quantities and $n$ denotes network quantities. When subscripts are dropped, $n$'s should be assumed.

### Mass conservation

Let $\theta$ be the volume fraction of a given phase, we then have trivially:

$$\theta_n + \theta_s = 1. \tag{1}$$

The incompressibility condition further yields:

$$\nabla \cdot (\theta_n \mathbf{v}_n + \theta_s \mathbf{v}_s) = 0. \tag{2}$$

Finally, conservation of network gives:

$$\frac{\partial \theta_n}{\partial t} = -\nabla \cdot (\theta_n \mathbf{v}_n) + J, \tag{3}$$

where $J$ is simply the net rate of network production by polymerization at a given location.

### Momentum conservation

Since only two forces act on the solvent, namely pressure gradients and drag due to relative motion of the network, the solvent momentum equation has a simple form:

$$-\theta_s \nabla P + H\theta_s\theta_n(\mathbf{v}_n - \mathbf{v}_s) = 0, \tag{4}$$

where $H$ is the solvent-network drag coefficient.

In addition to these terms, the network momentum equation must incorporate the forces that have been mentioned above (see Basic Concepts); namely, forces due to swelling, forces due to interaction with the membrane, and forces due to viscoelastic stresses:

$$\begin{aligned} &-\theta_n \nabla P - H\theta_s\theta_n(\mathbf{v}_n - \mathbf{v}_s) - \nabla \cdot \Psi^{nn} - \nabla \cdot \Psi^{nM} \\ &\quad + \nabla \cdot [\nu(\nabla \mathbf{v}_n + (\nabla \mathbf{v}_n)^T] + \mathbf{F}^{el} = 0. \end{aligned} \tag{5}$$

In this equation, $\Psi^{nn}$ is the stress (tensor) of the network due to interfilament forces, $\Psi^{nM}$ is the network-to-membrane interaction term, $\nu$ is the viscosity, and $\mathbf{F}^{el}$ is the elastic force due to deformations.

## Constitutive equations

A number of prescriptions are necessary to provide closure to the mass and momentum equations: these are the constitutive equations that establish the link between physical laws and biological behaviors.

### Network polymerization

We assume that the net rate of polymerization of network is determined by a logistics type of law:

$$J = \frac{\theta_n}{\theta_0}\frac{\theta_{eq} - \theta_n}{\tau_n}. \tag{6}$$

This formulation allows one to incorporate the idea that the rate of monomer release and addition should be proportional to the number of filaments. The equilibrium network concentration is given by:

$$\theta_{eq} = \theta_0(1+m). \tag{7}$$

Here $m$ is a dimensionless concentration of a polymerization messenger produced by the membrane with emissivity $\varepsilon_m$ (cm $s^{-1}$), lifetime $\tau_m$, and diffusion coefficient $D_m$ so that:

$$\frac{\partial m}{\partial t} = -\nabla \cdot (m\mathbf{v}_s) - \frac{m}{\tau_m} + D_m \nabla^2 m, \tag{8}$$

with appropriate von Neumann boundary conditions:

$$\mathbf{n} \cdot \nabla m = \frac{\varepsilon_m}{D_m}, \tag{9}$$

where $\mathbf{n}$ is the unit normal vector to the membrane. In general, we have chosen $D_m$ and $\tau_m$ such that the penetration depth $\sqrt{D_m \tau_m}$ is small; as a result $\theta_n = \theta_0$ for most of the interior of the cell. However, when the neutrophil is stimulated, the emissivity rises sharply in certain areas resulting in a localized increase in polymerization.

### Network-network interaction

In simulations of the swelling model described below (see Two Models: Network Swelling versus Polymerization Force), we have implemented an isotropic stress term proportional to the network concentration, i.e.:

$$\Psi^{nn}_{ij} = \psi^{nn}_0 \theta_n \delta_{ij}, \tag{10}$$

where $\delta_{ij}$ is the usual Kronecker symbol. If $\psi^{nn}_0$ is negative, one has a net contractility of the network (e.g., under the influence of myosin motors) while if $\psi^{nn}_0$ is positive, one has a repulsive pressure term that causes network swelling.

### Network-membrane interaction

If one assumes, as is the case in our polymerization force model, the existence of forces on the cytoskeleton normal to the membrane (i.e., no shearing stress), the network-to-membrane stress can be written:

$$\Psi^{nM}_{ij} = \psi^{nM} n_i n_j, \tag{11}$$

where $\mathbf{n}$ is the unit normal vector to the membrane, and where $\psi^{nM}$ will depend, among other things, on the distance to the membrane (i.e., far from the membrane one expects $\psi^{nM} \sim 0$). Essentially, this expression embodies a directional swelling (or contractile) stress acting in the network near the membrane. This has the basic effect of applying local pressure to the membrane. In the case of the polymerization force model, $\psi^{nM}$ naturally depends on the local polymerization rate as is described next.

### Implementation of the polymerization force model

We have used the simplest heuristic approach to a polymerization force term by making it linearly proportional to the local polymerization rate. In our calculations, the magnitude of the stress term is given by:

$$\psi^{\mathrm{nM}}=\psi_0^{\mathrm{nM}}\tau_{\mathrm{n}}J_{\mathrm{m}}=\psi_0^{\mathrm{nM}}\tau_{\mathrm{n}}\frac{\theta_{\mathrm{eq}}-\theta_0}{\tau_{\mathrm{n}}}\frac{\theta_{\mathrm{n}}}{\theta_0}=\psi_0^{\mathrm{nM}}m\theta_{\mathrm{n}}, \qquad (12)$$

where one will recognize $J_{\mathrm{m}}$ as the part of network polymerization that is due only and strictly to the messenger $m$.

From a thermodynamic point of view, one might prefer a form for this constitutive law involving the net polymerization ($J$) of the network rather than just the part related to the messenger. However, we have found that this leads to serious difficulties, as when $\theta_{\mathrm{n}} \rightarrow \theta_{\mathrm{eq}}$, the stress vanishes and the network concentration is frozen at its equilibrium value. Empirically, what happens in these simulations is that after a short transient, as the network concentration builds up, protrusion ceases with $J \rightarrow 0$.

Physically, this may be interpreted by postulating that the stimulated addition of monomers to the network occurs predominantly near the membrane, whereas disassembly happens further back without impediment to the Brownian ratchet or other propulsive mechanism.

### *Network viscosity and elasticity*

Whether the cytoskeleton must be treated as a viscous or elastic phase has been a longstanding matter of debate. Suffice it to say that from a physical standpoint, this depends on the relative magnitude of the strain rate to the cytoskeletal molecular remodeling rate. Both terms are considered in the present work. The viscosity is taken to be linearly dependent on network concentration:

$$\nu=\nu_0\theta_{\mathrm{n}}. \qquad (13)$$

The incorporation of an elastic stress term in our models involves material history and as such presents considerable technical challenges, especially in the presence of advection. The approach we have used here is a ''poor man's'' elasticity in the sense that it only accounts for compression and dilation through an isotropic stress term and ignores shear contributions. For this, we introduce the scalar field $w > 0$ that is evolved as follows:

$$\frac{\partial w}{\partial t}=-\nabla\cdot(w\mathbf{v}_{\mathrm{n}})+\frac{1-w}{\tau_{\mathrm{el}}}, \qquad (14)$$

where $\tau_{\mathrm{el}}$ is the decay time of elastic memory of the network related to the remodeling rate by the following ansatz:

$$\tau_{\mathrm{el}}=\frac{\tau_{\mathrm{n}}}{2}\frac{\theta_0}{\theta_{\mathrm{eq}}}. \qquad (15)$$

As one can see, $w$ is an advected cytoskeletal volumetric coefficient that is $<1$ if there has been recent dilation, $>1$ if there has been recent compression, and that decays back to 1 in isovolumetric flow. In a Maxwellian-like model, the elastic contribution to the momentum equation can then be written:

$$\mathbf{F}^{\mathrm{el}}=-\nabla\psi^{\mathrm{el}}=-\nabla[\psi_0^{\mathrm{el}}\theta_{\mathrm{n}}(w-1)], \qquad (16)$$

where $\psi_0^{\mathrm{el}}$ is a proportionality constant, the specific network stiffness.

### *Boundary conditions*

Boundary conditions have to be specified for both solvent and network phases. If we assume impermeability of the plasma membrane to both water and cytoskeleton, we have:

$$\mathbf{v}_{\mathrm{s}}\cdot\mathbf{n}=\mathbf{v}_{\mathrm{n}}\cdot\mathbf{n}=\mathbf{v}_{\mathrm{M}}\cdot\mathbf{n}, \qquad (17)$$

where $\mathbf{n}$ is the unit normal vector to the membrane and $\mathbf{v}_{\mathrm{M}}$ is the velocity of the membrane.

We further have to consider two possible types of boundary conditions: those that represent motion constrained by a solid surface such as that of a pipette, and those that represent free motion of the membrane. Solid walls impose the trivial constraint:

$$\mathbf{v}_{\mathrm{s}}\cdot\mathbf{n}=\mathbf{v}_{\mathrm{n}}\cdot\mathbf{n}=0, \qquad (18)$$

and depending on whether the boundary condition is stick or slip, $\mathbf{v}_{\mathrm{n}}\cdot\mathbf{t}$ will be required to vanish or not. Here $\mathbf{t}$ is the membrane tangent vector (well-defined in two dimensions). The solvent boundary condition is always taken to be slip.

For free boundaries, a condition of stress balance across the membrane has to be written by equating the internal stress tensor with external stresses (in the context of this work, these are limited to predetermined external pressures $P_{\mathrm{ext}}$) while taking into account the contribution of membrane surface tension. Adding Eqs. 4 and 5, and making use of the fact that all forces of interest are written in conservative form, we obtain the following:

$$\nu(\nabla\mathbf{v}_{\mathrm{n}}+(\nabla\mathbf{v}_{\mathrm{n}})^{\mathrm{T}})\cdot\mathbf{n}-\Psi\cdot\mathbf{n}-P\mathbf{n}=-2\gamma\kappa\mathbf{n}-P_{\mathrm{ext}}\mathbf{n}, \qquad (19)$$

where $\Psi$ is the full network stress tensor (including the contributions of ordinary swelling, directional force and elasticity), $\gamma$ is the surface tension, and $\kappa$ is the mean curvature of the membrane.

## Membrane surface tension

One of the main conclusions of the recent work of Drury and Dembo (2001) was that some sort of surface dilation viscosity is necessary to explain the time-dependence of neutrophil entry into a micropipette under aspiration (see Neutrophil Aspiration in a Micropipette). This was implemented by adding a term proportional to $\nabla_{\mathrm{M}}\cdot\mathbf{v}$ (where $\nabla_{\mathrm{M}}$ is the divergence along the plane tangent to the membrane) to the surface tension in the boundary momentum equation (Eq. 19) together with an equation for the evolution of membrane wrinkling. Practically, this meant that the surface tension was taken to increase locally in regions of surface creation.

In contrast, this study takes a simpler approach by considering the surface tension as a global property of the cell, as can be noted from the absence of a divergence term acting on $\gamma$ in Eq. 19. In a sense, this is a special case of what was done in Drury and Dembo (2001) as, instead of setting a specific

parameter for the diffusion of cortical stress, such diffusion is taken to be infinitely rapid. As a justification of this assumption, note that at the microscopic level, the plasma membrane is essentially inextensible and massless. Furthermore, the fluid mosaic nature of the bilayer allows it to act as a perfect conductor of stress (see Fig. 18). Thus a change in surface tension due to deformation in one region of the cell is instantly communicated to the entire plasma membrane. This global property of membrane tension is supported by the observations of Raucher and Sheetz (1999) in fibroblasts, and the results of Zhelev et al. (1996) that are described in this article's section Pseudopod Formations by fMLP Stimulation.

As has long been known (Schmid-Schönbein et al., 1980; Ting-Beall et al., 1993), the neutrophil is endowed with about double the membrane area needed to accommodate a spherical form. This spare membrane appears to be stored in small-scale wrinkles that can be unfurled as shape changes demand it (see Shao et al., 1998; Finger et al., 1996; Simon and Schmid-Schönbein, 1985; Petty et al., 1981). The energy cost of this unfurling represents a dynamic contribution to the surface tension. In the present work we have chosen the following form for the surface tension:

$$\gamma = \begin{cases} \gamma_0 & \text{if } \dfrac{dA}{dt} \le 0 \\ \gamma_0\left(1 + S\dfrac{dA}{dt}\dfrac{\tau_\gamma}{A_0}\right) & \text{if } \dfrac{dA}{dt} > 0 \end{cases} \tag{20}$$

where $A$ is the total surface area of the cell, $A_0$ is the area of the sphere of equivalent volume, and $\tau_\gamma$ is a relaxation time. The ''slack'' coefficient $S \in [0,1]$ is determined by the amount of slack available in the membrane before unfurling begins in earnest when the area becomes greater than a threshold value $A_s$. We have used the following ansatz:

$$S(A) = \begin{cases} 0 & \text{if } A < A_s \\ (A - A_s)/(A_0 - A_s) & \text{if } A_s < A < A_0 + 2(A_s - A_0). \\ 1 & \text{if } A > A_0 + 2(A_s - A_0) \end{cases} \tag{21}$$

In our work, $A_s = (1 + s)A_0$ where $s$, the threshold coefficient for surface viscosity, is 5%.

Of note is the absence of an elastic term in Eq. 20 for the surface tension (i.e., $\gamma$ depends linearly on $dA/dt$ rather than $A$). Such a term was taken into account by Drury and Dembo (2001) but found to have only a small importance in the pipette aspiration problem as long as the pipette is not too narrow. While there is no doubt that it is present and important at larger deformations than those considered here (e.g., see Needham and Hochmuth, 1992), we have chosen to neglect the elastic term to avoid adding yet another parameter to our models.

## Two models: network swelling versus polymerization force

One of the central issues of cell motility revolves around the origin of forces that are produced by the cytoskeleton according to the needs of the cell, especially in cases when there is no clear evidence that molecular motors are involved. It is important to recognize that how this issue is approached depends somewhat on whether one subscribes to a predominantly fluid versus elastic physical picture for the cytoskeleton.

In the fluid picture, the cytoskeleton is viewed as a highly dynamic structure that is continually recycled at a turnover timescale that is shorter than the prevalent strain rate. Arguments in favor of this are provided by in vitro studies such as those of Kuhlman et al. (1994) or Wachsstock et al. (1994) that show the turnover of a common actin crosslinker, $\alpha$-actinin, to occur on timescales of less than 1 s. In addition, in vivo studies of neutrophils (Cassimeris et al., 1990; Cano et al., 1991) and other amoeboid cells (e.g., Sund and Axelrod, 2000) have shown fast actin subunit cycling in and out of the polymerized state over the course of cell motion. The cytoskeleton is then conceived as a disorganized structure with isotropic properties, most notably when it comes to force generation.

In the elastic picture, the cytoskeleton is viewed as a more permanent, organized scaffolding that allows for the directional production of force. An example where this is clearly the case is given by the ultrastructure of skeletal muscle cells. The picture provided by electron-microscopy of neutrophils (Ryder et al., 1984) or other amoeboid cells is less clear, however; on the one hand, the very existence of a connected network of filaments gives credence to the idea of a degree of rigidity, but on the other hand, the apparent spatial disorganization of those structures argues for amorphous properties.

Those two pictures in turn lead to different ideas about the yet undetermined process of force generation in the absence of molecular motors. Since there is no preferred cytoskeletal direction in the cytoskeleton-as-a-fluid picture, the cytoskeleton is endowed with an isotropic equation of state that is devoid of memory terms. More concretely, since we know that actin polymers carry a large negative charge (isoelectric point 5.4; see also Xian et al., 1999) that will lead to interfilament repulsive forces, and also that thermal agitation of the network tends to lead to the least constrained configuration possible, it is reasonable to posit the existence of a swelling stress that tends to expand the cytoskeleton in regions where it is overdense. This has been used in the prior modeling studies of Dembo (1989) and He and Dembo (1997).

Within the ''cytoskeleton-as-scaffolding'' picture, the polymerization force model has gained increasing visibility over the last few years. The basic idea is that the free energy released by the addition of monomers to a filament is transduced to generate a pressure against a membrane that sterically interferes with the reaction, as observed, for instance, in the sickling of erythrocytes. Originally formulated by Hill and Kirschner (1982), the concept was revived in the form of a rectified Brownian ratchet mechanism (Peskin et al., 1993) to explain amoeboid cell motion (Mogilner and Oster, 1996). Other forms of network-membrane interactions

are possible, but our implementation of a membrane-cytoskeleton repulsion term that is dependent on polymerization rate should address those too (see Brownian Ratchets). From a phenomenological point of view, the main strength of the polymerization force model is that it allows for the directed application of force in cellular activities, while its principal weakness is that it lacks a clear answer to the question of how this level of directionality is maintained.

Because there is, as yet, no definitive evidence that indicates which approach is correct, we have chosen to present both in this study. It should be pointed out, however, that there are yet alternative views that are not considered here —for instance, the recent suggestion of prestressed network in the model for motility of *Listeria* of Gerbal et al. (2000), or other models of cellular motility involving molecular motors.

## Choice of parameters

From a computational point of view, the equations for both models are exactly the same with the difference between models stemming from a different choice of parameters intervening in the constitutive laws. In the case of the swelling model, the specific swelling stress $\psi_0^{nn}$ is nonzero while the polymerization force strength $\psi_0^{nM}$ and the specific network stiffness $\psi_0^{el}$ are both set to zero. Conversely, in the elastic/polymerization force model (sometimes equivalently labeled in this article as the polymerization-force model), $\psi_0^{nM}$ and $\psi_0^{el}$ are nonzero while $\psi_0^{nn}$ vanishes (see Table 1).

The parameters relevant to our calculations are listed in Table 1. It should be noted that their selection is the result of hundreds of numerical simulations that cannot be fully presented here. We will therefore limit ourselves to a brief discussion of each parameter in the light of biological plausibility. Further constraints can be found in the sections devoted to each experiment.

As indicated in Table 1, the parameters can be subdivided into those that affect cytoskeletal kinetics and those that deal with stresses. We discuss the former first.

### *Kinetics of network polymerization*

From a numerical standpoint, the baseline network density is almost arbitrary in the sense that coefficients such as specific network viscosity can easily be rescaled to provide the same momentum equation for different network concentrations. As it is, the cytoskeletal volume fraction in the passive neutrophil was taken to be $\theta_0 = 0.1\%$ (see estimates from Watts and Howard, 1993).

The network turnover and decay time was picked to be 20 s; such a timescale has been found to be appropriate, as argued in the section Two Models: Network Swelling versus Polymerization Force. A change by a factor of 2 either way does not change our results markedly. An upper limit is, however, provided by the time is takes for the neutrophil to extend a pseudopod (less than a minute). A lower limit is provided by the fact that the cytoskeleton appears to have a persistence timescale that is at least greater than a few seconds.

As mentioned in the section Constitutive Equations, network polymerization above and beyond the baseline equilibrium level is taken to be driven by a diffusible chemical messenger $m$ emitted by the membrane. This is of course not intended literally, but rather as a catch-all for a complicated collection of biochemical intermediates such as Arp2/3 and others (e.g., see Weiner et al., 1999; Machesky et al., 1997). Of note is that a similar approach was recently adopted by Rappel et al. (2002) in a sophisticated model of Dictyostelium polarization. The messenger is characterized by a lifetime $\tau_m$ and a diffusion coefficient $D_m$; those parameters can be rescaled by arbitrary factors with little change. However, when combined, they yield a penetration depth from the membrane $d_m = \sqrt{\tau_m D_m}$ that has critical physical importance, inasmuch as it defines the range of stimulation of polymerization.

In the case of the polymerization force model, only polymerization immediately next to the membrane contributes to protrusive forces. It is therefore reasonable to expect that the effective range of active polymerization from the area of stimulation should be small; for our calculations that distance is $\sim 0.3$ $\mu$m. A shorter distance would not be resolvable by the mesh, whereas from a purely utilitarian perspective, a larger distance would essentially waste the polymerization away from the membrane.

In the case of the swelling model, polymerization plays a role by increasing the network density in an entire compartment of the cell and thus generating a swelling stress. Thus strict localization is not needed except for the creation of thin structures. In the case of pseudopod formation, this corresponds to 1–2 $\mu$m so that we have set a diffusion distance $\sim 0.5$ $\mu$m.

Baseline membrane emissivity of the polymerizing messenger in the unstimulated neutrophil was taken to be small such that there is little excess cytoskeleton over the baseline network level $\theta_0$. Activation of the neutrophil causes an increase in network polymerization; in our calculations, this is mediated by an increase in emissivity by $\sim 2$ orders of magnitude at localized patches of the membrane. Specific values are discussed below with the presentation of our results for each of the experiments.

### *Stress parameters*

To set our stress parameters, we have made liberal use of the constraints obtained by Drury and Dembo (2001) in their experiments on passive neutrophil aspiration. A difference, however, is that our work does not include shear thinning. While there is little doubt that shear thinning does occur and is important in the dynamics of the neutrophil (e.g., see Tsai et al., 1993), introducing it enlarges the parameter space to

**TABLE 1 Parameters used in the simulations**

| Parameters and variables | Symbol(s) | Units | Swell model | Polymerization model |
|---|---|---|---|---|
| Neutrophil radius | $R_c$ | cm | $4.25 \times 10^{-4}$ | $4.25 \times 10^{-4}$ |
| Baseline network density | $\theta_0$ | – | $10^{-3}$ | $10^{-3}$ |
| Network decay time | $\tau_n$ | s | $2 \times 10^{1}$ | $2 \times 10^{1}$ |
| Messenger concentration* | $m$ | – | – | – |
| Equilibrium network | $\theta_{eq} = \theta_0(1 + m)$ | – | – | – |
| Messenger diffusion coefficient | $D_m$ | $cm^2\ s^{-1}$ | $3 \times 10^{-3}$ | $10^{-9}$ |
| Messenger decay time | $\tau_m$ | s | 1 | 1 |
| Messenger penetration depth | $d_m = \sqrt{D_m \tau_m}$ | cm | $5.5 \times 10^{-5}$ | $3.2 \times 10^{-5}$ |
| Baseline membrane emissivity | $\varepsilon_0$ | $cm\ s^{-1}$ | $10^{-5}$ | $10^{-5}$ |
| Stimulated emissivity† | $\varepsilon_s$ | $cm\ s^{-1}$ | $1.5 \times 10^{-3} - 8 \times 10^{-4}$ | $1.2 \times 10^{-3} - 2.4 \times 10^{-3}$ |
| Specific network viscosity‡ | $\nu_0$ | poise | $3 \times 10^6 - 6 \times 10^6$ | $3 \times 10^6 - 6 \times 10^6$ |
| Specific network swelling§ | $\psi_0^{nn}$ | $dyn\ cm^{-2}$ | $6 \times 10^6 - 3 \times 10^6$ | 0 |
| Polymerization force strength¶ | $\psi_0^{nM} d_M$ | $dyn\ cm^{-1}$ | 0 | $1.25 \times 10^{1}$ |
| Specific network stiffness | $\psi_0^{el}$ | $dyn\ cm^{-2}$ | 0 | $6 \times 10^6$ |
| Elastic decay time | $\tau_{el} = (\tau_n/2)\ (\theta_0/\theta_{eq})$ | s | – | – |
| Network-solvent drag | $H$ | $poise\ cm^{-2}$ | $1.6 \times 10^{11}$ | $1.6 \times 10^{11}$ |
| Static membrane tension‖ | $\gamma_0$ | $dyn\ cm^{-1}$ | $2.5 \times 10^{-2}$ | $2.5 \times 10^{-2}$ |
| Surface tension viscosity | $\gamma_0 \tau_\gamma$ | poise cm | $7.5 \times 10^{1}$ | $7.5 \times 10^{1}$ |
| Membrane viscosity threshold coefficient | $s$ | – | 5% | 5% |

*Maximum messenger concentration $m \sim 60$ when the neutrophil is stimulated.
†This is the maximum emission rate of polymerizing messenger for the Zhelev et al. (1996) and Usami et al. (1992) experiments, respectively.
‡The viscosity is doubled for experiments that involve fMLP stimulation. Macroscopic viscosity is $\nu \sim \nu_0\theta_0 = 3 - 6 \times 10^3$ poise $= 3 - 6 \times 10^2\ P_a$ s. Note that because of probable shear thinning effects, this estimate of the viscosity is only valid for strain rates $\sim 0.01\ s^{-1}$.
§Network swelling was set to $6 \times 10^6$ dyn $cm^{-2}$ for some aspiration calculations for better comparison with the elastic model which has an elasticity of $6 \times 10^6$ dyn $cm^{-2}$ (see text, 1 dyn $cm^{-2} = 0.1\ P_a$).
¶The dynamically relevant term is the network-membrane potential energy times its range $d_M$ (see Appendix).
‖1 dyn $cm^{-1}$ = 1 mN $m^{-1}$.

such an extent that we thought it preferable to ignore it for clarity of exposition. Instead, we have restricted ourselves to the modeling of experiments that all have comparable shear rates.

Cytoplasmic viscosity in the passive neutrophil has previously been estimated by Drury and Dembo (2001) to be 1000–6000 poise (100–600 $P_a$ s) which is also consistent with other experimental data (e.g., see Evans and Yeung, 1989; Hochmuth et al., 1993). In our models where only the network phase contributes to the cytoplasmic viscosity, the baseline viscosity $\nu_0\theta_0$ was found be fairly tightly constrained in the range 3000–6000 poise. One should note that the assumption of linear dependence of viscosity on network density may not be correct; it is not unreasonable to think that there might be increased cross-linking with densities leading to gelation. This was not explored in the calculations presented here.

The main difference between our two models lies with the mode of active force generation. The swelling model includes a baseline swelling stress of $\sim 3000$ dyn $cm^{-2}$ ($3 \times 10^{-3}$ atm or 300 $P_a$) for a network volume fraction of $\theta_0 = 10^{-3}$. From a purely thermodynamical point of view, this is within plausible limits since this corresponds to a energy density of 6 $k_B T$ per monomer incorporated in the network (see Appendix, Another Look at the Swelling Force). A formal justification of this value however would necessitate a detailed thermodynamic model of the cytoskeleton and the ambient solvent. In the present work, this magnitude is set by the constraints from the pseudopod experiments (see Pseudopod Formation by fMLP Stimulation), rather than fundamental principles.

The polymerization force model includes a network-membrane repulsive force that was determined empirically by the following constraints: the force should be as small as allowed without requiring an unduly high polymerization rate to produce active movement. The connection of the polymerization force strength with Brownian ratchet models is discussed in detail in Brownian Ratchets in the Appendix.

As discussed, the swelling force model views the cytoskeleton as an isotropic fluid and therefore, the elastic force term is set to zero. On the other hand, elasticity is crucial to the polymerization force model, since in the absence of a swelling stress it is required to prevent separation of the cytoskeletal and aqueous phases in circumstances such as aspiration of a neutrophil (see Elastic Force versus Swelling).

The solvent-network drag coefficient, $H$, is of order $1.6 \times 10^{11}$ poise $cm^{-2}$ as per the estimates of Dembo and Harlow (1986). It is worth noting that compared to the other terms in

the network momentum equation, its contribution is small, and that solutions are therefore not sensitive to its precise value.

The static surface tension of the cortical membrane has been measured by numerous experimentalists and has been found to be of order $2.5 - 3.5 \times 10^{-2}$ dyn cm$^{-1}$ or $2.5 - 3.5 \times 10^{-2}$ mN m$^{-1}$ (Evans and Yeung, 1989; Zhelev et al., 1996). The surface tension viscosity, $\gamma_0\tau_\gamma$, which expresses the increase in cortical tension under conditions of area dilation (see Membrane Surface Tension), was found by Drury and Dembo (2001) to be of order 100 poise cm (or 0.1 N m$^{-1}$ s) under a somewhat different model than the one used in this article. Using kinematic information from neutrophil aspiration, we have found the optimum value to be 75 poise cm for both the polymerization and swelling force models (see The Effect of Membrane Dilation Viscosity). Finally, it is apparent from experimental data that a small amount of membrane is immediately available for deformation as ''slack'' without inducing important dilation viscosity effects (see Membrane Surface Tension, Eqs. 20 and 21). This fractional amount $s$ is found to be 5% as described in Neutrophil Aspiration in a Micropipette and Pseudopod Formation by fMLP Stimulation.

### Numerical implementation

The simulations presented in this article were obtained by solving the model equations through a Galerkin finite element method using a mesh of quadrilaterals as described in Dembo (1994a), He and Dembo (1997), and Drury and Dembo (1999). Boundary conditions are as specified in the next section, Simulations of Experiments, for individual experiments.

Briefly, the calculation is advanced over a time-step $\Delta t$ determined by the Courant condition or other fast timescale of the dynamics. We evolve over $\Delta t$ by means of five sequential operations:

1. We advect the mesh boundary according to the network flow and then reposition mesh nodes for optimal resolution while preserving mesh topology, boundaries, and interfacial surfaces (Knupp and Steinberg, 1994).
2. We advect mass from the old mesh positions to the new mesh using a general Eulerian-Lagrangian scheme with upwind interpolation (Rash and Williamson, 1990).
3. We conduct diffusive mass transport and simultaneously carry out any chemical reactions. This is done according to a backward Euler (implicit) scheme coupled with a Galerkin finite element treatment of spatial derivatives and boundary conditions.
4. We use constitutive laws to compute necessary quantities such as viscosities and surface tensions.
5. Finally, the momentum equations and the incompressibility condition together with the applicable boundary conditions are discretized using the Galerkin approach and the resulting system is solved for the pressure, network velocity, and solvent velocity on the advected mesh using an Uzawa style iteration (Temam, 1979). Of note is that since we enforce a global surface tension $\gamma$ that depends on the rate of change of area $dA/dt$ (see Membrane Surface Tension), it was necessary to add a procedure that iterates between the velocity solution $v$ that depends on $\gamma$, and $dA/dt$ that depends on $v$, until all three are self-consistent.

The above computational cycle is repeated until the desired termination condition is reached (i.e., a prespecified evolution time, or a prespecified neutrophil behavior endpoint).

The cylindrical symmetry of the cases under consideration in this article allows the use of a two-dimensional mesh—some of the figures presented here simply correspond to recovery of the third dimension by rotation of the two-dimensional solution. Numerical convergence was confirmed by checking that the results were not sensitive to variations of the tolerance of the different iterations performed by the code as well as to variations of the spatial resolution.

Calculations were conducted using 64-bit arithmetic on a Linux PC workstation. The code was compiled with the Absoft Fortran 90 compiler. Post-processing was performed with a variety of publicly available software packages (SuperMongo, DISLIN, GMV, and ANA) as well as with customized code.

## SIMULATIONS OF EXPERIMENTS

### Neutrophil aspiration in a micropipette

This experiment has already been modeled by Drury and Dembo (2001) with a single-phase, viscous flow approach. Major differences in this study encompass the inclusion of two-phase flow, a different treatment of the cortical tension, the absence of shear thinning, and the addition of cytoskeletal swelling and elastic effects.

#### *Experimental findings*

Evidence related to aspiration experiments has already been thoroughly reviewed by Drury and Dembo (2001); we will therefore limit ourselves to a brief summary. Regardless of the details of the aspirating pressure or the pipette radius, neutrophil aspiration into a pipette takes place in three stages (see Fig. 1):

1. As aspiration begins an initial jump occurs during which the rate of entry of the neutrophil is rapid.
2. After ~10% of the cell volume is aspirated and the surface area has increased by ~5% from the initial spherical configuration, entry slows down to a nearly steady rate of entry that lasts for most of the aspiration time.
3. After ~60% of the cell volume is aspirated and the surface area has reached ~95% of its final value in the terminal 'sausage' configuration of the cell, the rate of entry accelerates markedly once again.

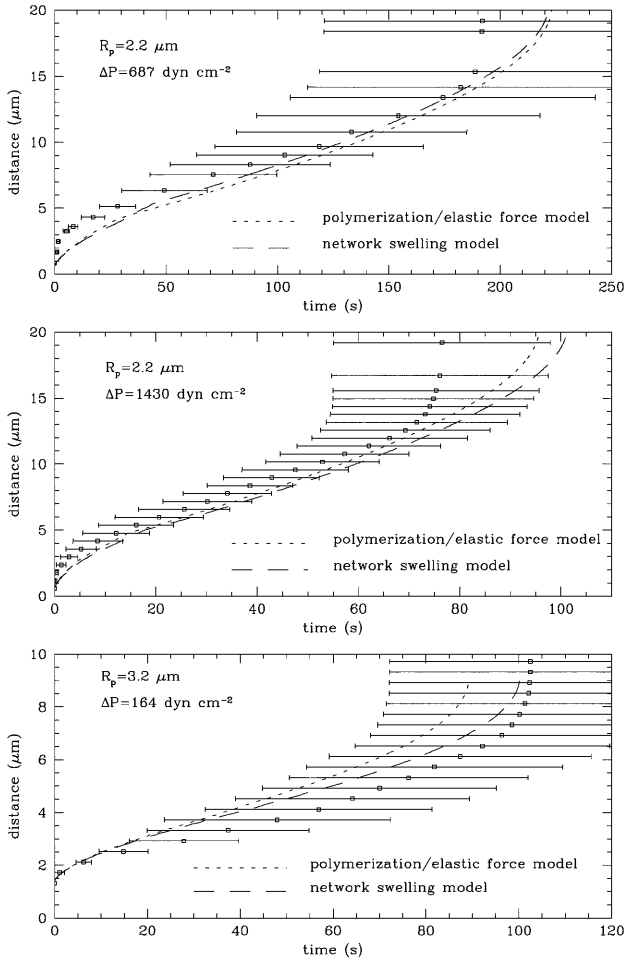


FIGURE 1 Distance of neutrophil entry versus time for three different experimental conditions. Squares and error bars represent data obtained by Drury and Dembo (2001).

From a morphological point of view, two findings are especially significant:

1. Throughout aspiration, the unaspirated portion of the neutrophil that remains outside the micropipette retains a shape that is close to semispherical, and does not show much flattening.
2. There does not appear to be marked phase separation between the cytoskeleton and the cytosol.

In addition to these qualitative findings, it is found that for a given pipette radius, the aspiration time $t_{asp}$ scales with the aspiration pressure $P_{asp}$ as $t_{asp} \propto P_{asp}^{-1.5}$. This naturally led Drury and Dembo (2001) to postulate shear thinning viscosity with an exponent of 0.5. As explained in the section called Stress Parameters, this is not implemented in the current calculations and for reasons of simplicity we have limited ourselves to conditions that all lead to similar shear rates.

### *Baseline simulations*

Initial conditions consisted of a spherical model neutrophil of radius $R_c = 4.25$ $\mu$m that was numerically relaxed for several virtual minutes in the absence of external forces to ensure chemical and dynamical steady state. As in Drury and Dembo (2001), the neutrophil was then considered to be in critical contact at the edge of a pipette of radius 2.2 or 3.2 $\mu$m and a negative pressure was applied to the portion of the free boundary within the pipette as given by Table 2. Boundary conditions at the pipette walls were assumed to be slip.

The basic results are shown in Table 2, and Figs. 1 and 2. Note first that the basic experimental features of aspiration, i.e., the three stages of the process enumerated above, the spherical nature of the outer part of the neutrophil, and the absence of significant phase separation, are all respected by the two models. In fact, differences between results obtained with either models are small, which is not surprising, inasmuch as this is an experiment in which there is no active production of force either by polymerization or by swelling.

### *Elastic force versus swelling*

It is worth noticing that the network concentration in the part of the neutrophil already within the pipette seen in Fig. 2 is somewhat less in the case of the polymerization force model than in the swelling model. An explanation for this is that, in the swelling model, the internal pressure of the network tends to equalize the network concentration regardless of prior history: overdense network pushes its way into the underdense pipette. On the other hand, in the polymerization force model, this must be achieved by elastic forces, which in certain conditions, fail to prevent phase separation.

If a small region $A$ (the tip of the aspirated part of the neutrophil) is depleted of network without the network in

**TABLE 2 Aspiration parameters and results**

| Model type | Pipette radius | Aspiration pressure | Aspiration time | Steady-phase velocity | Steady-phase surface tension |
|---|---|---|---|---|---|
| Experiment | 2.2 $\mu$m | 687 dyn cm$^{-2}$ | 192 s | $5 \times 10^{-2}$ $\mu$m s$^{-1}$ | ? |
| Elastic force | 2.2 $\mu$m | 687 dyn cm$^{-2}$ | 222 s | $5.6 \times 10^{-2}$ $\mu$m s$^{-1}$ | 0.13 dyn cm$^{-1}$ |
| Swelling force | 2.2 $\mu$m | 687 dyn cm$^{-2}$ | 221 s | $5.6 \times 10^{-2}$ $\mu$m s$^{-1}$ | 0.13 dyn cm$^{-1}$ |
| Experiment | 2.2 $\mu$m | 1430 dyn cm$^{-2}$ | 77 s | $1.2 \times 10^{-1}$ $\mu$m s$^{-1}$ | ? |
| Elastic force | 2.2 $\mu$m | 1430 dyn cm$^{-2}$ | 95 s | $1.3 \times 10^{-1}$ $\mu$m s$^{-1}$ | 0.25 dyn cm$^{-1}$ |
| Swelling force | 2.2 $\mu$m | 1430 dyn cm$^{-2}$ | 101 s | $1.3 \times 10^{-1}$ $\mu$m s$^{-1}$ | 0.25 dyn cm$^{-1}$ |
| Experiment | 3.2 $\mu$m | 164 dyn cm$^{-2}$ | 102 s | $4.5 \times 10^{-2}$ $\mu$m s$^{-1}$ | ? |
| Elastic force | 3.2 $\mu$m | 164 dyn cm$^{-2}$ | 90 s | $5.0 \times 10^{-2}$ $\mu$m s$^{-1}$ | 0.05 dyn cm$^{-1}$ |
| Swelling force | 3.2 $\mu$m | 164 dyn cm$^{-2}$ | 100 s | $4.6 \times 10^{-2}$ $\mu$m s$^{-1}$ | 0.04 dyn cm$^{-1}$ |

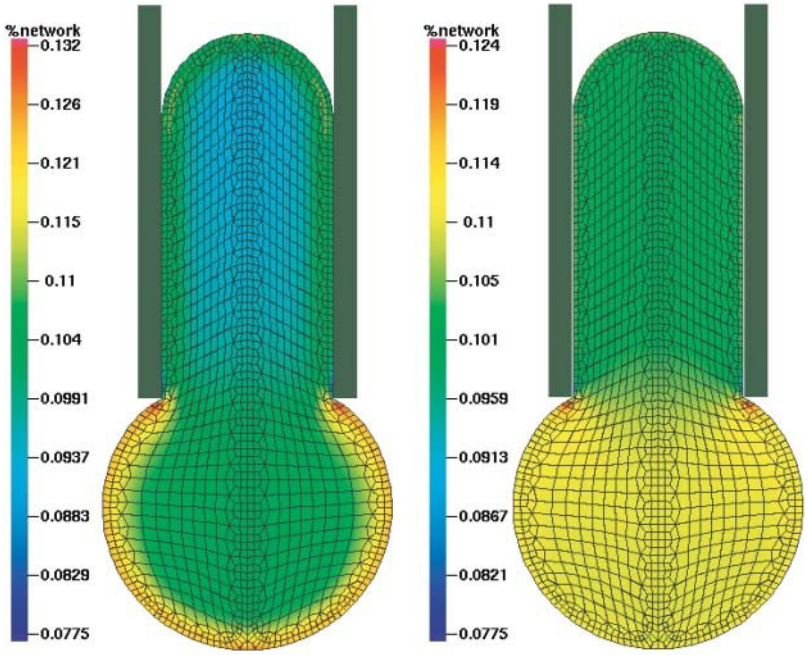


FIGURE 2 Neutrophil aspiration 55 s after beginning of entry (2.2-$\mu$m radius pipette, aspiration pressure of 1430 dyn cm$^{-2}$). Left corresponds to the polymerization/elastic force model and right corresponds to the swelling force model. Computational meshes are overlaid. Color represents the volume fraction of network.

region $B$ (the main cell body of much larger volume than $A$) being significantly compressed, we will have after the equation for elastic stress (Eq. 16):

In region $A$ : $\psi^{el} = \psi_0^{el}\theta_n(w-1) \sim 0$ since $\theta_n \sim 0$ (network depletion) even though $w \neq 1$ (network dilation),
In region $B$ : $\psi^{el} = \psi_0^{el}\theta_n(w-1) \sim 0$ since $w \sim 1$ (no deformation) even though $\theta_n \sim \theta_0$.

As a result, for $\psi_0^{el}$ below a critical value, elastic stress is too small to prevent phase separation. Once it occurs, phase separation will then progress due to the difference in viscosity that makes the flow of solvent much easier than the flow of network.

Consider for instance Fig. 3, which depicts simulations where the specific network stiffness and the specific network swelling were halved with respect to the baseline parameter. Runaway phase separation is evident in the elastic force model, whereas it remains negligible in the swelling force model. In addition to not having been observed, it should be noted that, should phase separation occur, it would work strongly against the final acceleration during the aspiration, as a solid plug of network would be slower to aspirate at the end of the process.

This leads us to the following conclusion: our baseline specific network stiffness $\psi_0^{el} = 6 \times 10^6$ dyn cm$^{-2}$ is close to the minimum possible if one assumes that swelling stresses do not play an important role. On the other the hand, the aspiration curve changes little for a range of specific network swelling parameters $\psi_0^{nn} = 10^6$ to $6 \times 10^6$ dyn cm$^{-2}$ (data not shown).

### *The effect of membrane dilation viscosity*

As argued by Drury and Dembo (2001), the shape of the aspiration curve argues toward a strong component of surface dissipation, inasmuch as simple viscous droplet models cannot account for the three stages of neutrophil aspiration. Dilation viscosity resisting the gradual unfurling of the cortical membrane, as the shape of the neutrophil changes from a ball into a sausage, provides a natural explanation for these features.

If one posits that the membrane is responsible for most of the resistance to aspiration, the initial jump of the neutrophil at the beginning of aspiration leads one to postulate the existence of a certain amount of slack that allows a small (5%) surface increase before dilation viscosity kicks in. This is illustrated in Fig. 4, which shows the difference between early entry curves with and without slack. Furthermore, pertaining to pseudopod growth, we shall see in Pseudopod Formation by fMLP Stimulation that there is experimental evidence supporting this finding.

Fig. 5 shows the central importance of the dilation viscosity in determining the rate of entry during the steady phase of aspiration. Indeed, we find that, for the 2.2-$\mu$m radius pipette with 1430 dyn cm$^{-2}$ aspiration pressure, the entry velocity varies almost strictly linearly with the dilation viscosity: at 100 poise cm, it is 0.096 $\mu$m s$^{-1}$; at 75 poise cm, it is 0.128 $\mu$m s$^{-1}$; and at 50 poise cm, it is 0.174 $\mu$m s$^{-1}$. Additional support is provided by power balance during the steady phase. Total power dissipation can be computed from the work of the aspiration pressure on the neutrophil:

$$\dot{W}_P = v_{asp} A_{pip} P_{asp}, \tag{22}$$

where $A_{pip}$ is the area of the pipette. The energy dissipation through unfurling of the neutrophil membrane can be written:

$$\dot{W}_\gamma = \dot{A}_{cell\gamma}, \tag{23}$$

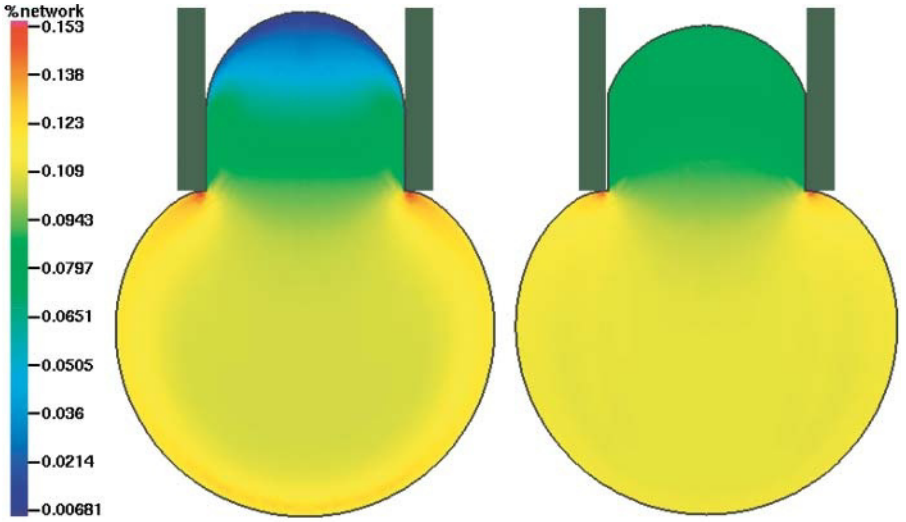


FIGURE 3 Neutrophil aspiration 8 s after beginning of entry for decreased specific network stiffness $\psi_0^{el} = 3 \times 10^6$ (*left*) and decreased specific network swelling $\psi_0 = 3 \times 10^6$ (*right*) (2.2-$\mu$m radius pipette, aspiration pressure of 1430 dyn cm$^{-2}$). Phase separation is apparent in the elastic/polymerization force model (*left*).

where $A_{cell}$ is the total neutrophil surface area and $\gamma$ is the effective surface tension including dilation viscosity effects. Fig. 6 provides the relevant quantities for one aspiration calculation in which one finds: $\dot{W}_P = 2.8 \times 10^{-9}$ ergs s$^{-1}$ and $\dot{W}_\gamma = 2.2 \times 10^{-9}$ ergs s$^{-1}$. Thus, in this case, the major part (80%) of energy dissipation in resistance to aspiration is contributed by membrane dilation with the balance principally due to cytoskeletal viscosity and compression.

### *The effect of cytoskeletal viscosity*

Fig. 7 shows entry curves comparing the baseline swelling model calculation to a model with increased network viscosity $(\theta_0\nu_0 = 3000\,\text{poise} \rightarrow \theta_0\nu_0 = 4000\,\text{poise})$ and decreased surface dilation viscosity $(\gamma_0\tau_\gamma = 75\,\text{poise cm} \rightarrow \gamma_0\tau_\gamma = 25\,\text{poise cm})$. It is remarkable that, although the aspiration times are about the same in both calculations, the shapes of the entry curves are significantly different. In particular, the final acceleration is absent and even replaced by a deceleration in aspiration!

Fig. 8 shows the details of cytoskeletal flow at the nozzle of the pipette for both types of models. When surface viscosity dominates, the taut cortex directs the flow of cytoskeleton around the edge of the pipette; velocity shears and variations in network concentration remain small (Fig. 8, *top*). On the other hand, when interior viscosity dominates, the cytoskeleton gets hung up at the edge of the pipette inlet, the local network concentration increases dramatically, and the velocity shears become important (Fig. 8, *bottom*).

At the end of aspiration, the requirement for additional surface area decreases as an ever smaller remaining sphere needs to be stuffed into the pipette. When the dominant term resisting aspiration is the surface dilation viscosity, this naturally leads to an acceleration. On the other hand, when cytoplasmic viscosity dominates, there is a slowdown of entry

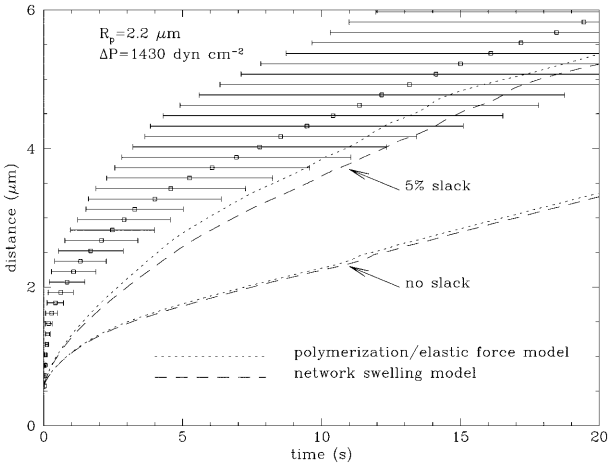


FIGURE 4 Detail of the initial jump phase of neutrophil entry versus time for various parameter choices.

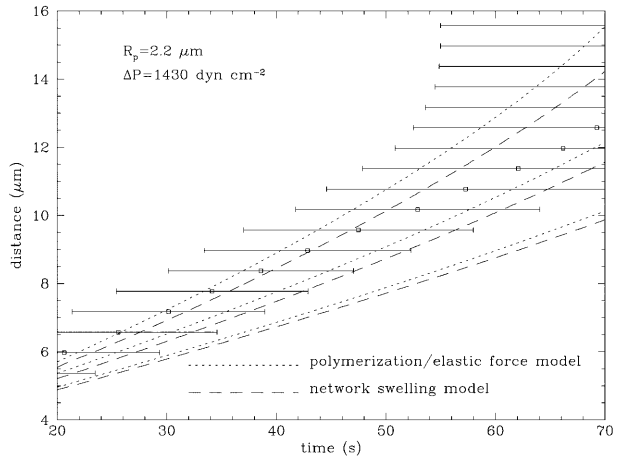


FIGURE 5 Detail of the steady phase of neutrophil entry for low surface tension viscosity (*upper pair of curves*), baseline surface tension viscosity (*middle pair of curves*), and high surface tension viscosity (*lower pair of curves*). Note that 1 poise = 0.1 $P_a$ s.

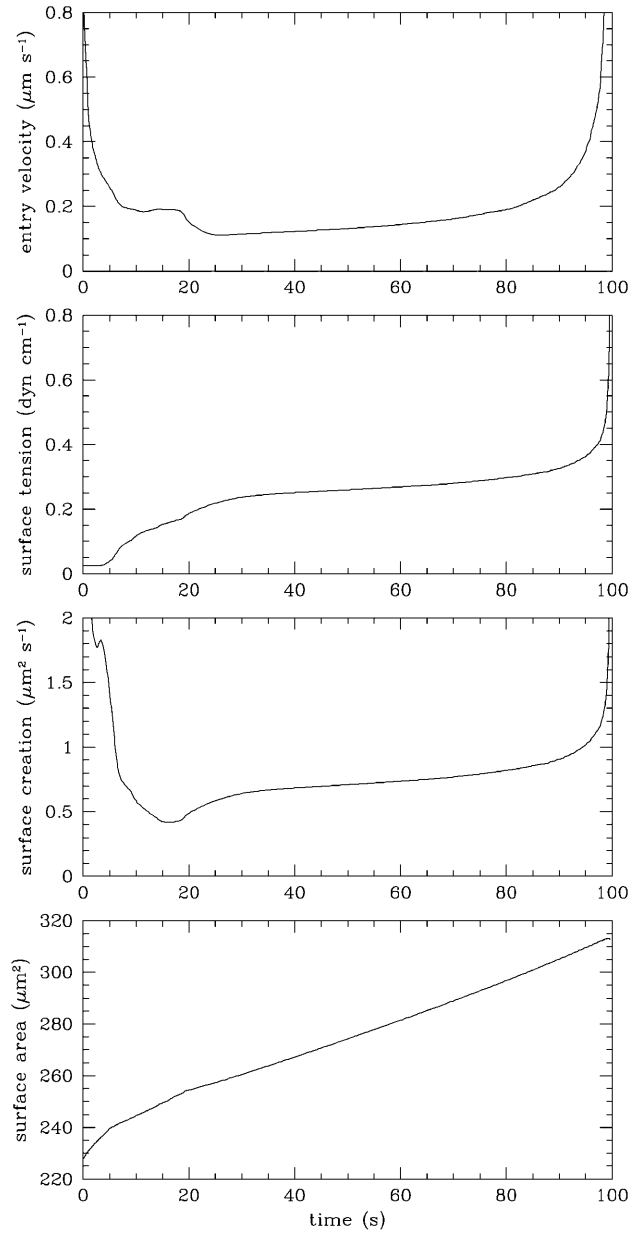


FIGURE 6 Surface area, surface creation rate, surface tension, and entry velocity as a function of time for the swelling force model (2.2-$\mu$m radius pipette, aspiration pressure of 1430 dyn cm$^{-2}$). Note that the final few seconds of the aspiration are subject to numerical errors that make the precise values of derivative quantities such as surface area creation rate and surface tension uncertain due to resolution problems near the entrance of the pipette.

toward the end of aspiration because the final dense residue of cytoskeleton in the remaining outside portion of the neutrophil tends to form a viscous plug that is hard to aspirate (Fig. 8).

We conclude that, for the conditions encountered in this article, 3000 poise (300 $P_a$ s) is an upper limit to cytoplasmic viscosity in the inactivated neutrophil (higher and lower viscosities are possible at lower and higher shear rates due to

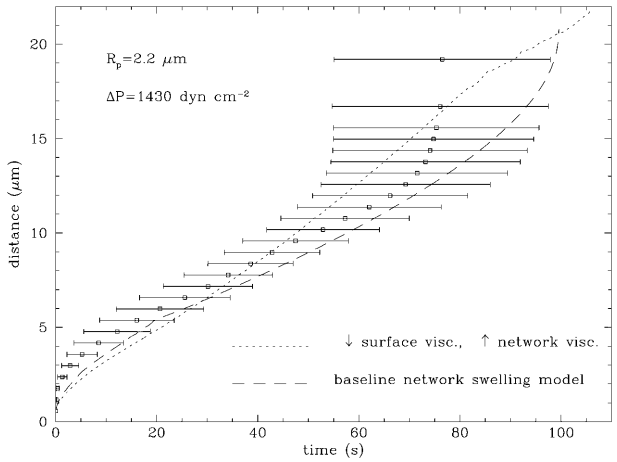


FIGURE 7 Comparison of numerical simulations of a model with baseline parameters and a model with increased network viscosity (↑33%) and decreased surface dilation viscosity (↓67%) (2.2-$\mu$m radius pipette, aspiration pressure of 1430 dyn cm$^{-2}$).

shear thinning). As to a lower limit of cytoplasmic viscosity, it is provided by aspiration data in 3.2-$\mu$m radius pipettes. Because these larger pipettes require less deformation for entry, cytoplasmic viscosity plays a more important role in

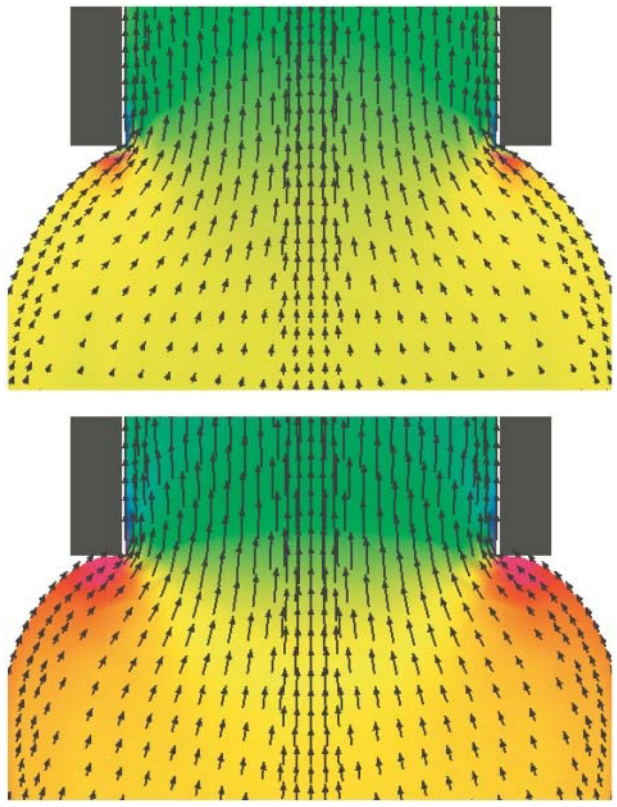

FIGURE 8 Comparison of numerical simulations of a model with baseline parameters (*top*) and a model with increased network viscosity (↑33%) and decreased surface dilation viscosity (↓67%, *bottom*) (2.2-$\mu$m radius pipette, aspiration pressure of 1430 dyn cm$^{-2}$). Color indicates network concentration, and arrows indicate network flow velocity field.

resisting aspiration (as already noted by Yeung and Evans, 1989). Viscosities significantly less than 3000 poise lead to unacceptably short aspiration times (data not shown).

## Pseudopod formation by fMLP stimulation

In a series of technically challenging experiments, Zhelev et al. (1996) have characterized aspects of the response of neutrophils to the chemoattractant fMLP. Using a pipette with gentle suction to maintain a neutrophil in place, they exposed a local region of the antipodal side of the cell to minute quantities of fMLP delivered by another micropipette (Fig. 9). They then observed the growth of a pseudopod extending toward the source of fMLP and were also able to simultaneously measure the cortical tension with the holding pipette by a law of Laplace method (Evans and Yeung, 1989). This study provides a remarkable probe of a cellular shape-changing process that is not dominated by surface boundary constraints.

### *Experimental findings*

The essence of the results of Zhelev et al. (1996) is illustrated in Figs. 9 and 10 (*bottom graph*). One will note the following salient features:

1. Noticeable growth of a pseudopod extending toward the fMLP source begins approximately 20–30 s after beginning of the exposure. It proceeds at a velocity $\sim$0.1 $\mu$m s$^{-1}$ for several tens of seconds before slowing down and/or stagnating. After a period of varying length (sometimes several minutes), the pseudopod retracts into the cell at a velocity somewhat less than the original extension speed.
2. Cortical tension initially remains at the baseline value of 0.025 dyn cm$^{-1}$ (= 0.025 mN m$^{-1}$), and only begins to increase after the pseudopod is several $\mu$m in length. It then rises rapidly $\sim$sixfold. Subsequently it returns to near baseline as soon as the pseudopod stagnation or retraction phase has been reached, well before the pseudopod has been resorbed.
3. The foremost 2 $\mu$m of the pseudopod is devoid of granules, probably indicating a region of high F-actin cytoskeletal density.
4. Initially, the morphology of the cell remains relatively spherical with a straight pseudopod extruding; during stagnation or retraction, the pseudopod thickens and the cell appears to become somewhat ovoid (prolate).

### *Baseline simulations*

As for the aspiration experiments, initial conditions consisted of a relaxed spherical model neutrophil of radius $R_c = 4.25$ $\mu$m. Throughout the simulation, we impose the condition $\mathbf{v} = 0$ at the antipodal point to the stimulation area, thus numerically mimicking the role of the holding pipette. As described below, enhanced emission of the diffusing polymerizing messenger is assumed to take place near the area exposed to fMLP, thereby leading to a local increase in network concentration.

The main results are shown in Figs. 9–12. Note first that the gross experimental findings are largely recovered; namely, that the pseudopod dimensions and morphology correspond to what is observed, and that we have indeed a frontal plug of dense cytoskeleton at the leading edge of the pseudopod.

Perhaps most interesting is that the surface tension behaves in the appropriate way in light of the fact that the corresponding parameters (slack, dilation viscosity) were fully determined by the aspiration experiments (see The Effect of Membrane Dilation Viscosity). Upon closer inspection, this is not surprising. Consider a cylindrical pseudopod of radius $R_{pod} = 1.5$ $\mu$m and extension velocity $v_{pod} = 0.1$ $\mu$m s$^{-1}$. The

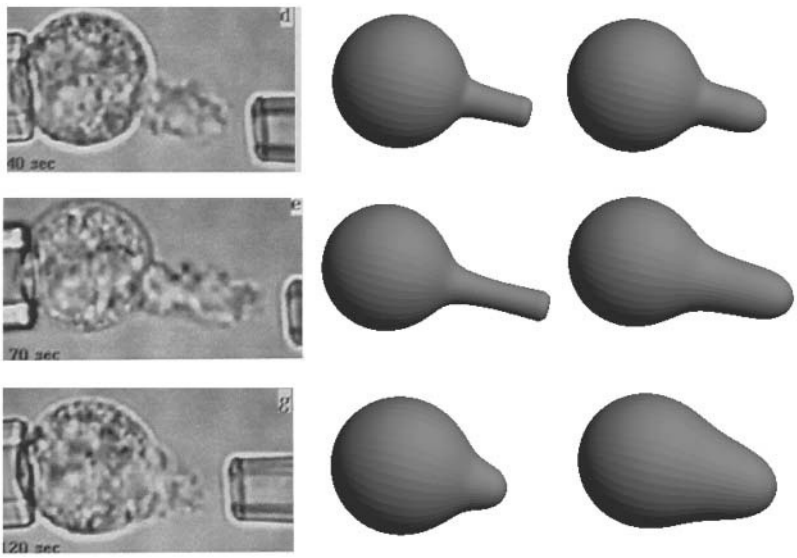


FIGURE 9 Microphotographs of a neutrophil being held by a pipette and extending a pseudopod toward the right where another micropipette is dispensing fMLP (*left*; from Zhelev et al., 1996; courtesy R. Hochmuth, copyright, Wiley-Liss). Computed time series of shapes for a polymerization force model (*center*) and a swelling force model (*right*).

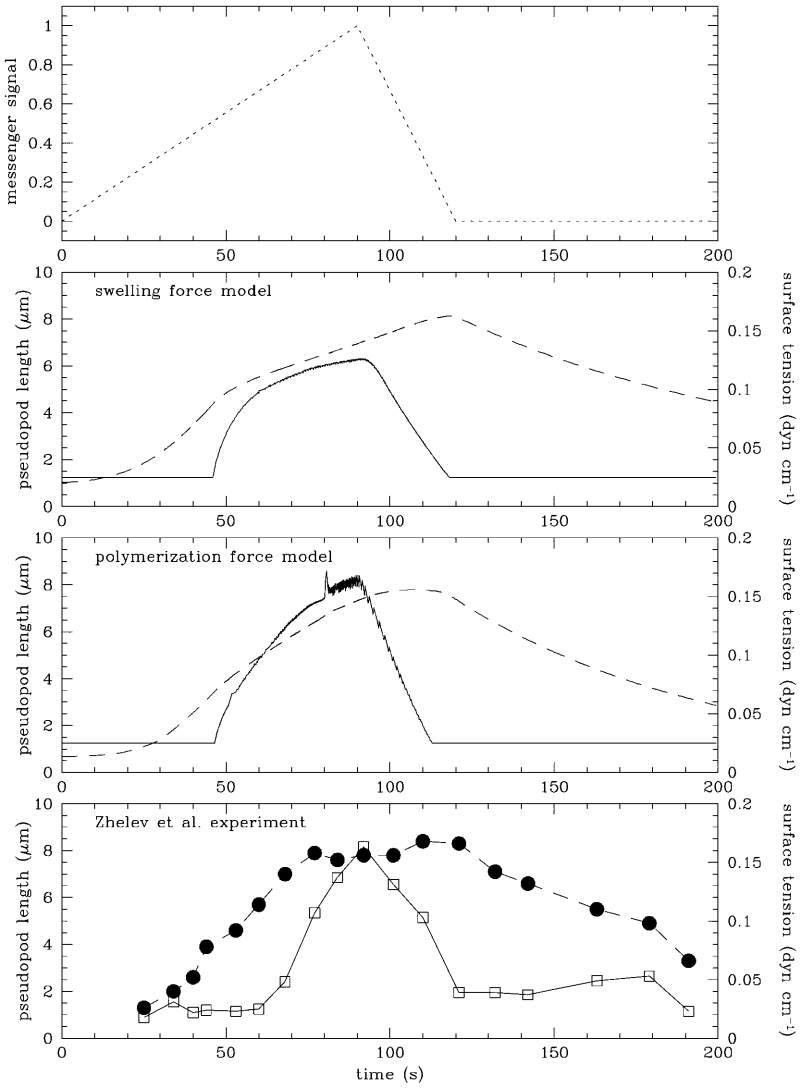


FIGURE 10 Distance of pseudopod extension (*dashed lines*) and cortical tension (*solid lines*) versus time for the stimulation of a neutrophil with fMLP. Bottom panel is the data from Zhelev et al. (1996), second panel shows result from the polymerization force model, and third panel shows results from the swelling model. Top panel shows the time course of the excitatory polymerizing messenger signal (normalized). Note that 1 dyn $cm^{-1} = 1$ mN $m^{-1}$.

rate of increase of the area of the pseudopod is $\dot{A}_{pod} = 2\pi R_{pod} v_{pod} \sim 10^{-8}\,cm^2\,s^{-1}$. Knowing the total area of the cell $A_c = 4\pi R_c^2$ and the dilation viscosity as determined in the section called The Effect of Membrane Dilation Viscosity, the effective surface tension is found to be ~0.3 dyn $cm^{-1}$. While this is of the right order of magnitude, this is clearly an overestimate, since this analysis neglects the shrinkage in area of the main cell body as cytoplasm is transferred to the pseudopod. A similar approach also shows that for a slack parameter of 5% of the total cell area, surface tension will only begin to rise when pseudopod extension reaches a threshold of a few $\mu$m.

### *The central role of the polymerization signal*

Since force production in our two models relies on the creation of network at precise locations in the cell, it should be obvious that how this occurs will be key to the characteristics of pseudopod extension. As discussed in Kinetics of Network Polymerization, the models include a polymerization messenger that is produced at the membrane and diffuses inside the cell with a finite lifetime. This is, of course, not to be taken literally; i.e., there undoubtedly is a complex pathway involved, but this approach has the benefit of simplicity and of encompassing some of the basic realities of such signaling: external stimuli are sensed at the external face of the membrane and converted to cytoplasmic signals through enzymatic activity at the internal face of the membrane. Ultimately, this all boils down to three issues: the spatial extent of the signal, the temporal course of the signal, and the intensity of the signal.

In our calculations, the way by which network creation is locally induced is through increased emission of the polymerization messenger at a defined patch of membrane. For the polymerization force model, the region of emitting membrane was taken to be a cap of curvilinear radius 0.75 $\mu$m from the symmetry axis while, on the other hand, for the swelling force model this was taken to be a cap of radius

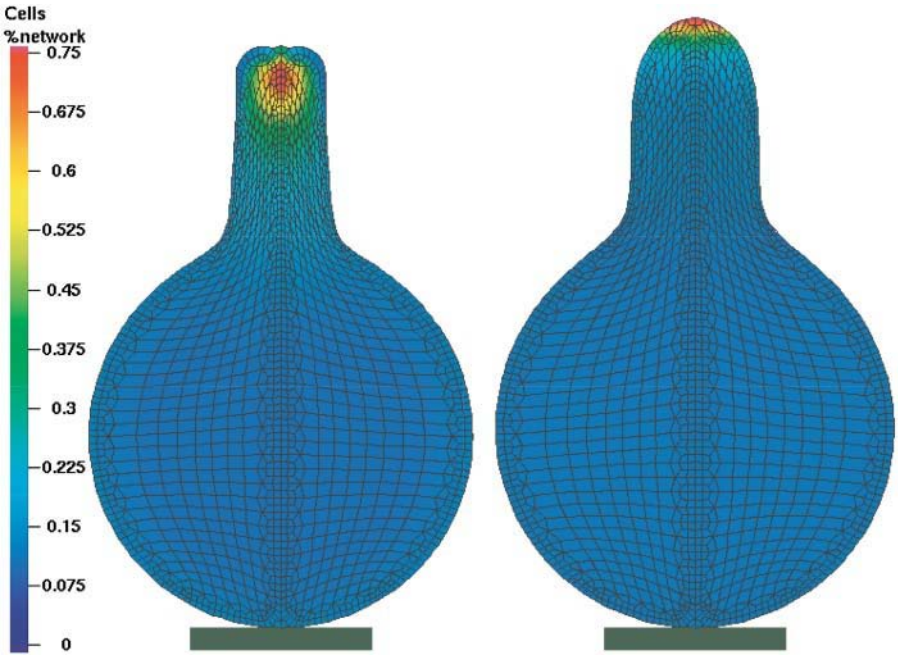


FIGURE 11 Calculation 60 s after fMLP stimulation. Left corresponds to the polymerization/elastic force model and right corresponds to the swelling force model. Computational meshes are overlaid. Color represents the volume fraction of network. The solid bar at the base is 4-$\mu$m long.

0.5 $\mu$m. The main constraint in setting those dimensions was provided by the girth of the pseudopod. In the case of the network swelling model, the application of force is more diffuse, and this is why a smaller area of activation is required.

The time-dependence of the polymerization was set to approach the temporal behavior shown in Fig. 10 (*bottom*). As can be seen, the cortical tension becomes maximum after 90 s of stimulation and returns to near baseline 30 s later. From a qualitative point of view, this indicates that the driving force of pseudopod extension goes from zero to a maximum and back to zero in the same timeframe, and that presumably, the polymerization signal does the same. As the simplest possible guess, we have chosen to assume a linear variation of the messenger emission as shown in Fig. 10. The free parameter of the maximum value of the messenger emission was then adjusted to give an approximately correct pseudopod maximum length.

### *Impact of the cytoskeletal viscosity*

In the absence of an unmovable external element to counteract protrusive force, network viscosity plays a key role in enabling the extension of a pseudopod. The basic idea is that

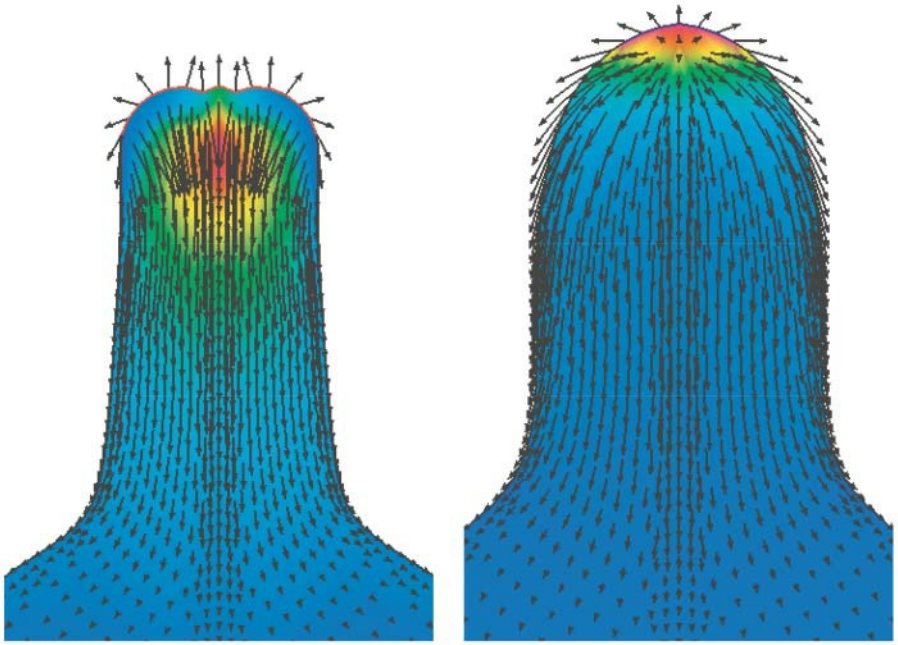

FIGURE 12 Detail of the pseudopod network velocity field at 60 s for the polymerization force model (*left*) and the swelling force model (*right*). Color indicates network concentration. The stimulatory part of the membrane is highlighted. Note the disjoining flow in the polymerization force model (*left*) versus the explosionlike flow in the swelling force model (*right*).

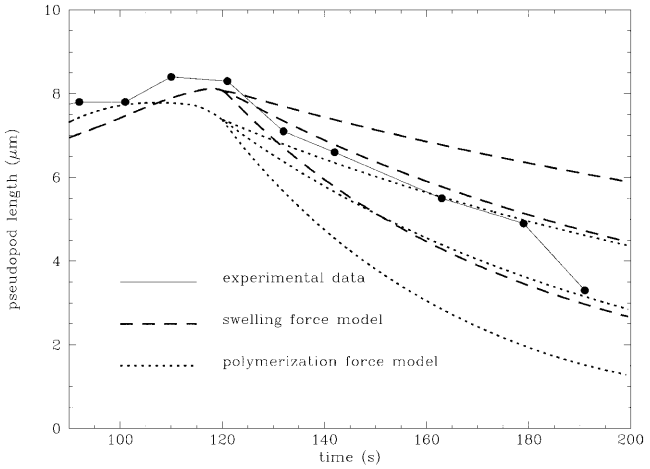


FIGURE 13 Retraction of the pseudopod versus time for varying viscosities ($1.2 \times 10^4 - 6 \times 10^3 - 3 \times 10^3$ poise). Note that 1 poise = 0.1 $P_a$ s.

as outward force somehow develops (through polymerization, swelling, or otherwise), bracing is provided by the viscosity of the network that prevents inward expansion and forces outward protrusion. However, for the purpose of a quantitative determination of the viscosity, it is preferable to focus on the subsequent recovery phase for which the confounding factors of putative swelling, elastic, and polymerization forces play less of a role.

The key assumption that is made here is that pseudopod retraction is a mostly passive process for which the principal determinants are the cortical tension (which is measured by Zhelev et al., 1996) and the network viscosity. This is defensible in light of the fact that the timescale for retraction of the pseudopod is of the same order of magnitude as the time for recovery of a passive, elongated neutrophil back to a spherical shape after pipette aspiration and expulsion (Tran-Son-Tay et al., 1991). Note that active depolymerization is not necessary for pseudopod retraction. In both models, the interruption of polymerization leads to a rapid decay of protrusive force, and even without allowing depolymerization, retraction proceeds according to viscosity and surface tension. That is not to say that active depolymerization does not occur, but the details of the biochemical kinetics cannot be constrained with the data at hand.

Fig. 13 shows the time course of pseudopod retraction for both models with varying specific viscosity $\nu_0 = 3 \times 10^6 - 6 \times 10^6 - 1.2 \times 10^7$ poise (effective viscosity is $\sim\theta_0 = 10^{-3} \times$ these values). Clearly, $\nu_0 = 6 \times 10^6$ gives the best fit to the data. This value is double what was deduced from the aspiration experiments (see The Effect of Cytoskeletal Viscosity) and may possibly be interpreted as the consequence of increased network cross-linking due to neutrophil activation. This increased viscosity was also necessary in our modeling of the activated neutrophil crawling in a micropipette (see Active Motion of a Neutrophil Inside a Micropipette). Finally, it is notable that Bathe et al. (2002) have recently also found that fMLP stimulation apparently increases the internal viscosity of neutrophils.

### *The swelling force model*

The key parameter of this model is the specific swelling $\psi_0^{nn}$, which was poorly constrained by the aspiration experiment (see Elastic Force versus Swelling). Let us first try to estimate it from first principles. As in this article's section Baseline Simulations, consider a cylindrical pseudopod of radius $R_{pod}$; assuming perfect bracing, i.e., no inward motion of the network, the $PdV$ work of expansion of the network for a pseudopod lengthening $\Delta l$ is $W_\psi = \psi_0^{nn}\theta_n \pi R_{pod}^2 \Delta l$. Similarly the surface tension work is $W_\gamma = \gamma 2\pi R_{pod}\Delta l$. Setting the two equal for $R_{pod} = 1.5$ $\mu$m and $\gamma = 0.15$ erg cm$^{-2}$ one obtains a minimum value $\psi_0^{nn}\theta_n = 2 \times 10^3$ dyn cm$^{-2}$. Assuming the network concentration is, at most, $\theta_n \sim 10^{-2}$ this leads to $\psi_0^{nn}\theta_n = 2 \times 10^3$ dyn cm$^{-2}$. This is a strong lower limit since we have neglected the viscous work and the inefficient nature of the viscous bracing of the pseudopod which leads to expansion forward and backward.

An upper limit to the value of $\psi_0^{nn}$ is provided by the existence of a dense area of cytoskeleton at the tip of the pseudopod. Note first $\tau_\psi = \nu_0/\psi_0^{nn}$ represents the dissipation timescale of network density perturbations. Should we have $\tau_\psi \ll \tau_p$, i.e., much less than the polymerization time, the network will expand faster than it can be built up by polymerization and a region of significantly overdense network will fail to appear. For this reason we have $\psi_0^{nn} < 6 \times 10^6$ dyn cm$^{-2}$.

In summary, the parameter constraints on the specific swelling $\psi_0^{nn}$ are:

- A lower bound is set by the requirement that the protrusion force be sufficient while keeping the network volume fraction to a level within reasonable limits.
- An upper bound is set by the requirement that the network be able to develop an appreciable density contrast with respect to the background without immediate dissipation through expansion.

For our calculations of the pseudopod extension, $\psi_0^{nn} = 3 \times 10^6$ dyn cm$^{-2}$ yields the best results while still remaining consistent with the aspiration computations.

### *The polymerization force model*

Quantitative analysis of the dynamics of the polymerization force as we have implemented it is conceptually nontrivial and for this reason, it is deferred to Appendix (Brownian Ratchets) where connection is made with Brownian ratchet models. We will here focus on basic physical arguments. Let us first point out that unlike in the swelling model, the existence of an overdense region of cytoskeleton is no longer a significant constraint; since there is no swelling force, overdense regions dissipate only by depolymerization and

not by expansion. The main constraints are set by the necessity of producing sufficient protrusive force while not having to drive polymerization to a point where unrealistically high network concentrations appear in the pseudopod.

From these demands we have derived a polymerization force strength $\psi_0^{\mathrm{nM}} d_{\mathrm{M}} = 2.5 \times 10^2$ dyn cm$^{-1}$ which requires a peak network concentration $\theta_{\mathrm{n}} \sim 0.015$.

## Active motion of a neutrophil inside a micropipette

In an elegant experiment that is a natural extension to studies of aspiration, Usami et al. (1992) have examined the active motion of neutrophils crawling inside a narrow pipette toward a chemoattractant. The beauty of the method is that by applying varying degrees of counterpressure one is able to rigorously quantify the amount of force generated by the neutrophil. As a result, this provides a ready-made test for continuum mechanical models of the neutrophil. One can only regret that there have, as yet, been no published attempts to expand this type of study further.

### *Experimental findings*

Using the chemoattractant fMLP, Usami et al. (1992) induced neutrophils to enter fibronectin-coated micropipettes of radius ~2.5 $\mu$m. They then continued to supply fMLP to the neutrophils thus prompting further advance into the micropipette while they varied an opposing counterpressure. Their results can be summarized as follows:

1. With no counterpressure, the progression velocity is approximately 0.33 $\mu$m s$^{-1}$.
2. Progression stops for approximately 16–20 cm $H_2O$ ($1.8 \times 10^4$ dyn cm$^{-2}$ or $1.8 \times 10^3$ $P_{\mathrm{a}}$) of counterpressure. Incidentally, this is close to the pressure drop in human capillaries.
3. The velocity varies approximately linearly with counterpressure.
4. There exists a frontal layer of thickness ~2−3 $\mu$m that is devoid of granules and is likely made up of dense cytoskeleton. At the same time, the rear of the cell appears to behave as a passive component that is dragged along by the frontal motor element.

### *Baseline calculations*

Initial conditions consisted of a model neutrophil (with volume corresponding to a sphere of 4.25 $\mu$m radius) inside a cylindrical pipette of radius 2.5 $\mu$m. The boundary conditions at the pipette wall were set to be stick for the forward 60% of the length of the neutrophil and slip for the remaining 40% as an approximate model for the passive rear of the cell. The frontal free boundary of the neutrophil was subjected to counterpressure as prescribed by Eq. 19. As in the modeling of the pseudopod experiment (see Pseudopod Formation by fMLP Stimulation), frontal polymerization of network is induced by emission of a polymerizing messenger at the part of the membrane exposed to fMLP (see below for the details).

The essence of our results is illustrated by Figs. 14–16, and is compatible with the observations of Usami et al. (1992). The reader will be able to verify that the rate of progression versus counterpressure is in agreement with experimental data and that one indeed recovers an approximately linear dependence of velocity on pressure. Furthermore, a dense region of cytoskeleton is evident at the front of the cell.

From a physical point of view, the mechanism of advancement of the cell against a load is similar for either the polymerization force or network swelling models. By action and reaction, frontal protrusive force leads to a retrograde flow of network. This flow transduces the protrusive force to the walls of the pipette via viscous dissipation thus allowing forward translocation of the cell. Such a mechanism is exactly analogous to the raking process hypothesized to take place in the lamella of crawling amoeboid cells (Dunn, 1980; Dembo and Harris, 1981).

### *The polymerization signal*

As stated before, a diffusing messenger emitted by the membrane determines the kinetics of network polymerization in our calculations (see Kinetics of Network Polymerization). In the Usami et al. (1992) experiment, the front portion of the neutrophil membrane covering the lumen of the pipette is exposed to fMLP. As for the Zhelev et al. (1996) experiment, we posit enhanced emission of polymerizing messenger in that area. We also posit that the emission is normalized to the surface area, i.e., that the total emission of messenger remains independent of the deformations of the surface within the lumen.

In addition, for the swelling model, we posit that the area of the membrane of the model cell which is adhering to the pipette and within 2 $\mu$m of the forward contact line also has an enhanced emission of polymerizing messenger. This is plausible to the extent that cell adhesion may be a trigger of polymerization in itself. Evidently, such a process would make less sense in the polymerization force model where the application of force against a solid boundary would have no clear purpose.

### *Calibration of stress parameters*

Since several parameters interact to cause forward motion, we have found it illuminating to call upon a simplified flow model to try to get a handle on the features that determine cellular behavior in this experiment. One can write, as a very crude approximation, for the cell velocity $v$:

$$v = \frac{-\alpha \Delta P + \varepsilon F}{\nu_{\mathrm{c}}}, \tag{24}$$

where $\alpha$ is a geometric coefficient, $\Delta P$ is the counterpressure applied to the cell (negative for suction), $F$ is a measure of the motile protrusion force, $\varepsilon$ is an efficiency factor of conversion

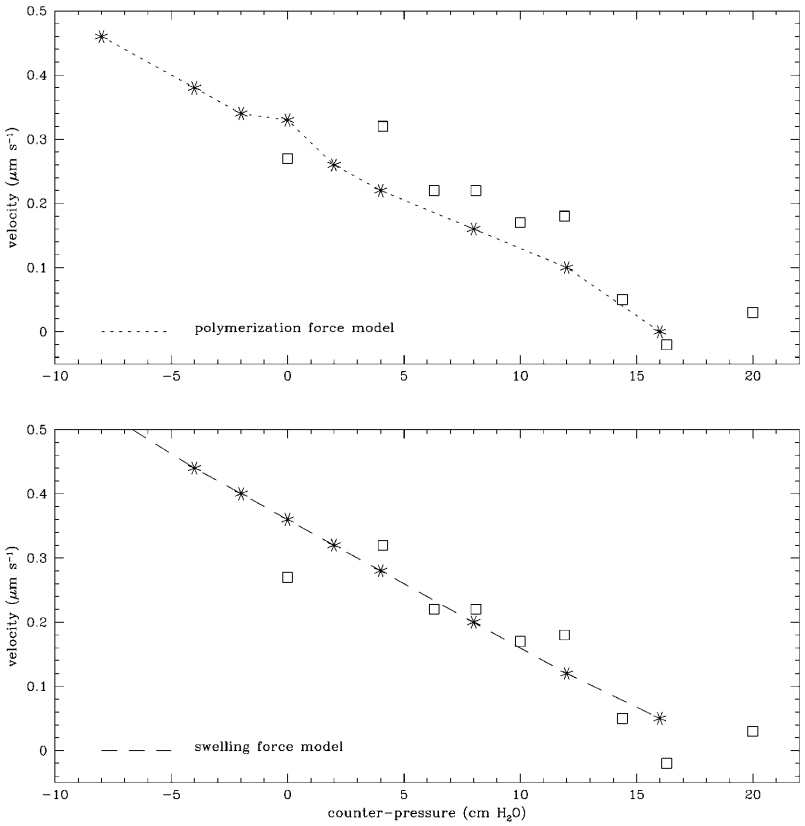


FIGURE 14 Velocity of neutrophil progression versus counterpressure in a 2.5-$\mu$m radius pipette. Squares represent experimental data from Usami et al. (1992) and stars are computed values from both numerical models.

of force to forward velocity, and $\nu_c$ is a global average of cellular viscosity.

If the protrusion force is set to zero, one simply recovers Poiseuille's law for viscous flow in a pipe. If the counterpressure is set to zero, the second term determines the motion. Because force and viscosity are both proportional to network density $\theta_n$, the behavior of the efficiency factor $\varepsilon$ is important in the determination of

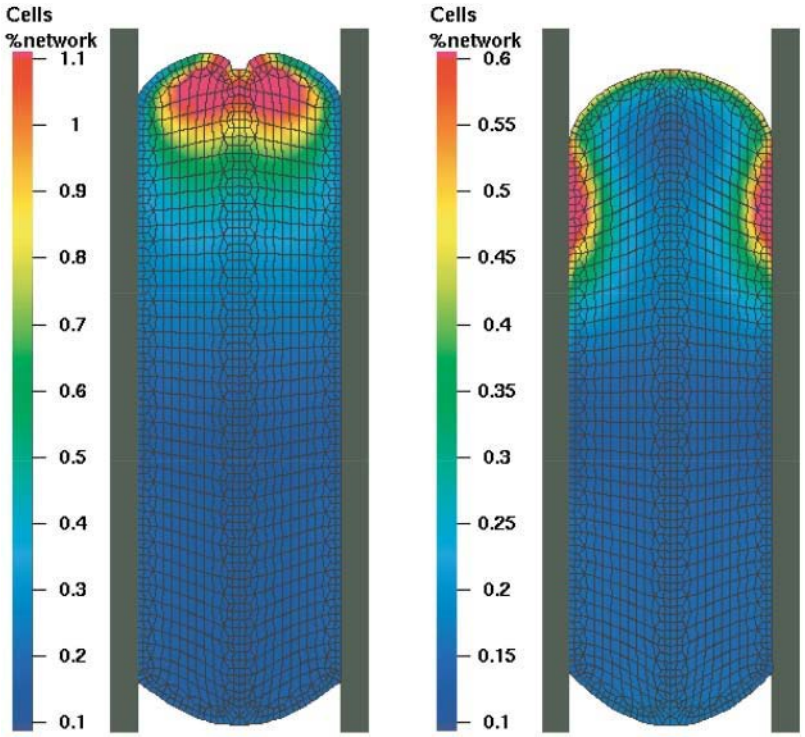


FIGURE 15 Neutrophil progression inside a 2.5-$\mu$m radius pipette without counterpressure. Left corresponds to the polymerization force model and right corresponds to the swelling force model. Computational meshes are overlaid. Color represents the volume fraction of network.

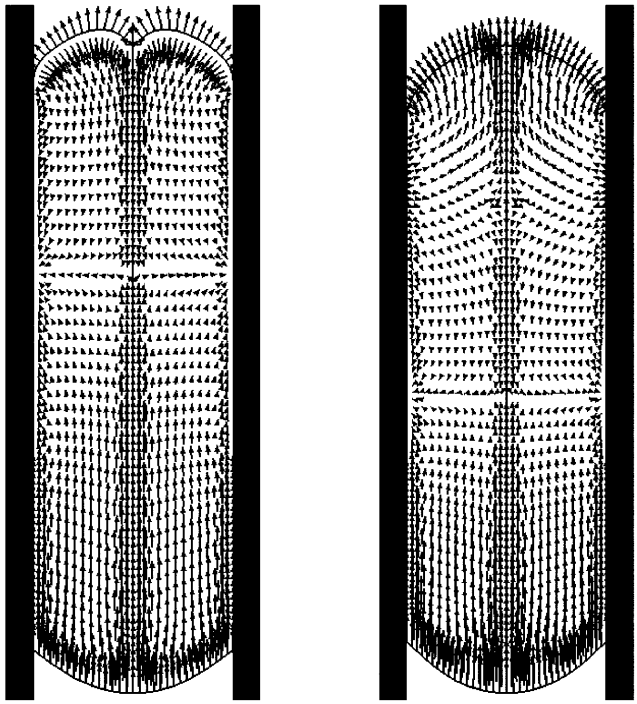

FIGURE 16 Cytoskeletal network velocity field for neutrophil progression inside a 2.5-$\mu$m radius pipette without counterpressure. Left corresponds to the polymerization force model and right corresponds to the swelling force model.

velocity. For instance, we evidently have $\lim_{\nu\to 0}\varepsilon = 0$, since in the absence of viscosity, no stress can be transported to the walls. In any case, if one assumes that $\varepsilon$ remains approximately constant for a range of counterpressure (an assumption that is sometimes incorrect, as we will show later), one sees that:

The slope of the velocity pressure curve is principally determined by the overall viscosity of the cell. We will thus have $\nu_c = \alpha P_{stall}/v_0$ where $v_0$ is the velocity with zero counterpressure.

Once the overall viscosity $\nu_c$ of the cell and therefore, the slope of the pressure-velocity line is fixed, the required production of force is determined by the value of $v_0$.

Similar to what was the case for the pseudopod extension experiments, it was found necessary for both models to have specific cytoskeletal viscosity of $\nu_0 = 6 \times 10^6$ poise corresponding to a baseline viscosity $\nu_0\theta_0 = 6 \times 10^3$ poise (600 $P_a$ s). Lower viscosities such as the one used for the aspiration simulations led to either a stall pressure that was too low, or too high a velocity at zero counterpressure (data not shown). For this given viscosity, and for each of our two models, the swelling force and polymerization force strengths that gave appropriate velocities at zero counterpressure were found to be consistent with the parameters determined in the pseudopod extension simulations.

### *Instabilities at the frontal membrane*

A finding of our numerical experiments is that for high counterpressures, and especially near the stall pressure, the frontal free surface of the neutrophil becomes unstable and is liable to buckle (Fig. 17). This occurs in both polymerization and swelling force models, and, although we are in the creeping flow regime, it is somewhat reminiscent of the behavior observed in Rayleigh-Taylor instabilities (heavy fluid over light fluid). Of note is that there is some mention by Usami et al. (1992) of neutrophils occasionally detaching from one side of the pipette, but details are scant.

A detailed analysis of those instabilities is beyond the scope of this article, and in any case needs to be performed in three spatial dimensions to be accurate—one more than available from our calculations. However, we will here list the factors that have stabilizing and destabilizing influences.

### *Stabilizing factors*

1. Surface tension resists increases in surface area caused by rippling of the interface.
2. Viscous stress resists shears that are necessary to buckle the membrane.

### *Destabilizing factors*

1. Since the polymerization signal is emitted by the membrane, inward-directed convexity decreases polymerization and inward concavity does the reverse. The increased network in outward projections with the decreased network around invaginations leads to enhancement of the instability.
2. The existence of a front-to-back negative gradient of network density means that invaginations see less and less viscoelastic and/or swelling resistance as they deepen into the cell.

To a large extent, the destabilizing factors can be neutralized by prescribing a constant density plug of network at the front few $\mu$m of the cell, or equivalently increasing the diffusion range of the polymerization messenger to a much larger length. However the problem then becomes that it is impossible to obtain a narrow pseudopod in the Zhelev et al. (1996) experiment (see The Central Role of the Polymerization Signal).

### *Aspiration of actively crawling neutrophils*

Our calculations clearly show that for the polymerization force model the velocity pressure curve has an inflection point at small negative counterpressures (i.e., for suction). This is not seen for the swelling force model for which the slope of the velocity pressure curve remains essentially constant (see Fig. 14). We have observed such a difference between the two models for all the parameter choices (viscosity, swelling, and

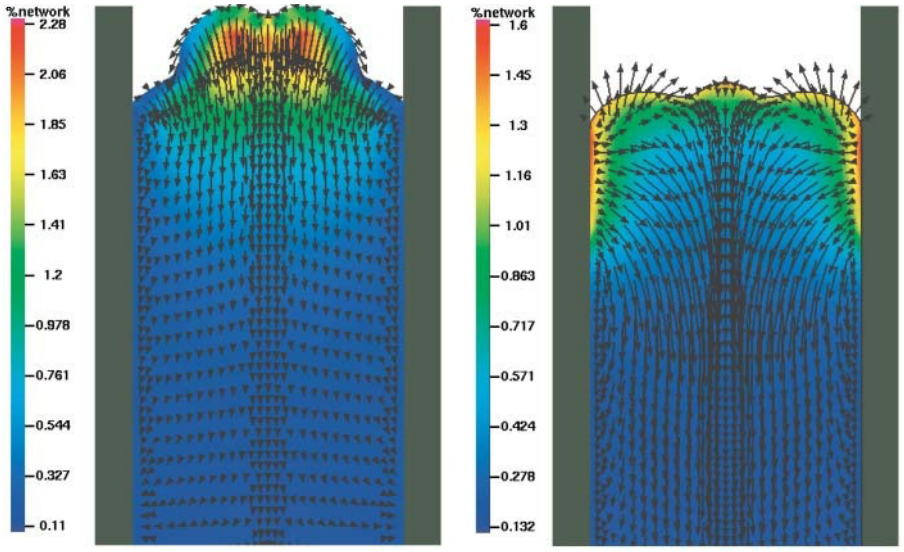


FIGURE 17 Cytoskeletal network velocity field for neutrophil progression inside a 2.5-$\mu$m radius pipette against 16 cm of $H_2O$ counterpressure. Color scale represents volume percentage of network. Left corresponds to the polymerization force model and right corresponds to the swelling force model.

polymerization force strength, pipette radius, etc.) that we have tested.

This behavior can be explained qualitatively by the fact that in the polymerization force model, protrusive activity depends on network-to-membrane repulsion. When suction is applied, the viscoelastic stress on the cytoskeleton tends to pull the network back from the frontal membrane, thus decreasing the strength of the interaction (especially since network polymerization is proportional to network density). Note that this is completely consistent with the Brownian ratchet model, predicting that protrusive force decreases as the membrane sterically interfering with the polymerization reaction is unloaded.

Referring to the simple model of Eq. 24, the effect amounts to a sudden decrease in the force term as one transitions from positive to weakly negative counterpressure. For stronger suction, one recovers the initial slope determined by overall cellular viscosity. The inflection of the velocity-pressure curve does not occur in the swelling model because the locus of force production is diffuse and the magnitude of the protrusive force is only weakly dependent on the precise distribution of network in the frontal compartment of the cell.

Unfortunately, Usami et al. (1992) limited their investigations to positive counterpressures only. It is, however, clear that an extension of their experiment to include aspiration pressures could be a powerful discriminant of the mode of force production in crawling neutrophils.

## DISCUSSION

### Packaging neutrophils: control of cortical tension

We have argued in this article that the experimental data suggests the existence of a surface dilation viscosity that increases surface tension when membrane is recruited from folds and villi to accommodate deformations of the neutrophil. From an evolutionary point of view, this is a beautiful solution to a demanding set of functional specifications. In the course of their life in the circulation, neutrophils are required to squeeze into capillaries ~60% of their diameter several hundred, if not thousand, times. This has to occur without disturbing the neutrophil's lethal payload of toxic granules that can easily cause inflammatory disasters if it is not discharged in the right circumstances. At the same time, the cost in terms of vascular resistance to blood flow must be minimized; in other words, the quiescent neutrophil must flow easily in and out of capillary vessels. The solution to this conundrum: a highly viscous shrink-wrap with thinning that shifts the stress of deformation to the neutrophil's surface, away from the dangerous inner cargo (see The Effect of Cytoskeletal Viscosity).

The physical implementation of this mechanism remains mysterious and for that matter, the magnitude and origin of membrane surface tension itself remains controversial. Experimental investigations of surface tension generally fall into two categories. The law of Laplace method pioneered by Evans and Yeung (1989) measures a macroscopic cortical tension by determining the threshold pressure for flow into a micropipette. This method reports a tension 0.025–0.035 dyn $cm^{-1}$ (or 0.025–0.035 mN $m^{-1}$) in the quiescent neutrophil for which the relative contributions of the cytoskeletal cortex and the membrane are unknown.

The tether method (e.g., see Heinrich and Waugh, 1996; Shao et al., 1998; Raucher and Sheetz, 1999; Hochmuth and Marcus, 2002) measures the force required to pull a thin membranous tether from the cell (or vesicle as the case may be). For quiescent neutrophils, the threshold force is approximately $F_t = 5 \times 10^{-6}$ dyn = 50 pN (Shao et al., 1998), and this is consistent with the force needed to hold an extended tether (Volkmar Heinrich, private communication). Because the tethers are very thin, this is likely to reflect a pure membrane tension instead of a cytoskeletal contribution. Evidently, the

radius of the tether is not known but if one assumes a membrane tension $\gamma \sim 0.03$ dyn cm$^{-1}$, then $F_t = 4\pi R_t \gamma$ (Hochmuth et al., 1996) leading to a tether radius $R_t \sim 0.15$ $\mu$m. This is at the upper limit of acceptable (per microscopic observations of the tethers), so that it is unlikely that pure membrane tension is significantly lower than the Laplace value.

It has been shown (Evans and Rawicz, 1990; Rawicz et al., 2000) that in the case of giant bilayer vesicles, thermal undulations can contribute to the macroscopic surface tension (see also Marsh, 1997 and references therein). Alternatively, Schmid-Schönbein et al. (1995) have proposed that cortical tension was due to a spontaneous resting curvature of membranes. However, in both pictures, the tension becomes a state function of surface area that does not obviously depend on the dilation rate.

The fact that surface viscosity appears to be only effective during dilation and not during shrinkage is probably indicative of an irreversible process that breaks the bonds that stabilize the membrane reservoir in folds and villi. Of note is that these stabilizing bonds cannot simply be focal staples (see Fig. 18, *top*) which would allow the fluid membrane to flow around them. Rather, they must reflect diffuse membrane-to-membrane or membrane-cytoskeleton-membrane interactions (Fig. 18, *bottom*). The latter hypothesis is supported by the numerous experiments that have shown an apparent decrease in surface tension with exposure to cytochalasin (Tsai et al., 1994; Finger et al., 1996; Raucher and Sheetz, 1999).

If one assumes that the cartoon depiction of the bottom panel of Fig. 18 is valid, the formalism of Dembo (1994b; see also Dembo et al., 1988), developed to address relationships between peeling tension and peeling velocity through a thermodynamic model of cell adhesion, is applicable with minimal adjustments. In that work, it was found that for large peeling tensions, $T_{peel}$:

$$v_{peel} \propto \left(\frac{T_{peel}}{T_{crit}}\right)^{q} \ln \frac{T_{peel}}{T_{crit}}, \tag{25}$$

where $q$ is $>1$ for slip bonds and $\leq 1$ for ideal bonds. For a net dilation of macroscopic cell area $\dot{A}_{cell} > 0$, this translates into:

$$\dot{A}_{cell} \propto \left(\frac{\gamma}{\gamma_0}\right)^{q} \ln \frac{\gamma}{\gamma_0}. \tag{26}$$

If the logarithm is weakly varying, for $q = 1$ (ideal bonds), one recovers the linear behavior posited by our model. For $q > 1$, meaning slip bonds that are easier to break with increasing tension, one obtains the dilation viscosity thinning that is not modeled in this article but is necessary to fit experimental data at widely different aspiration rates (Drury and Dembo, 2001).

The formalism of Dembo et al. (1988) also predicts that the critical tension $\gamma_0$ at which no unfurling of membrane occurs is related to the number of binding sites per unit area of membrane $n_b$ in the following manner:

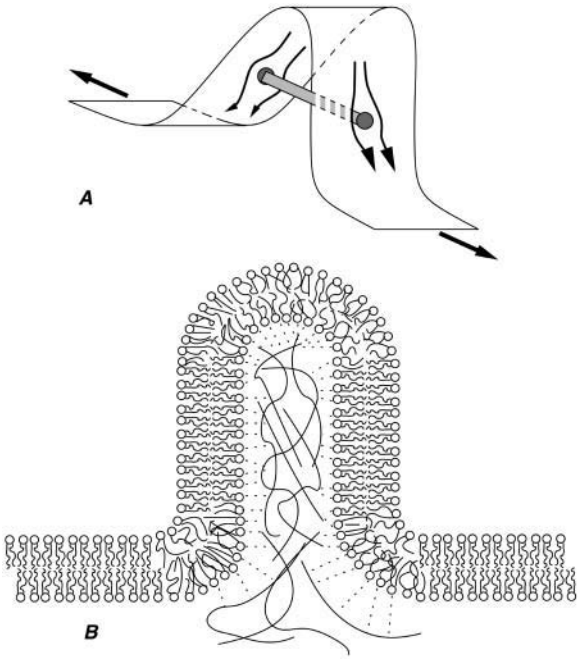


FIGURE 18 Lipid bilayer folds: (*A*) Flow of bilayer around a solitary transfold staple. (*B*) Stabilization by membrane-network-membrane interaction.

$$\gamma_0 = O(k_B T n_b). \tag{27}$$

For $\gamma_0 = 0.025$ dyn cm$^{-1}$, this gives $n_b = O(5000)$ sites per $\mu$m$^2$ of membrane.

It should be pointed out that although Eq. 26 applies to a single fold, in reality, recruitment of membrane takes place by the simultaneous unfurling of many folds all over the cell. Further, one would expect that in the ensemble of membrane-storing folds, the least cohesive region contributes first, then the second least cohesive, and so on. In such a process may reside the explanation for the 'slack' that initially allows rapid area expansion with little increase in tension.

## Maintaining and restoring the shape of neutrophils

### *Viscous, elastic, and swelling forces*

It has long been noted that while the cytoplasm of passive neutrophils generally appears to behave as a viscous fluid, in rapid deformations, there can be a memory effect that tends to return it to its original shape (e.g., see Zahalak et al., 1990, and Tran-Son-Tay et al., 1991). It has also been noted that this restoring force disappears after the neutrophil has been held in its new configuration for a while (10 s). In the context of single phase models, this fading memory phenomenon led to the idea that the cytoplasm has Maxwellian properties, i.e., that it is endowed with a decaying elasticity. The decay time would then be determined by the remodeling timescale of the cytoskeleton. It has also been suggested that displacement and deformation of the nucleus might be responsible (Kan et al., 1999).

In the two-phase picture of the cytoplasm as it is presented in this article, an alternative explanation for this decaying memory effect is possible. Since cytoskeletal and cytosolic density can vary in tandem, a rapid deformation of the neutrophil can lead to regions of network overdensity and underdensity. For instance, in the case of a poking experiment, a bow wave of network accumulates ahead of the poker. If one then postulates a cytoskeleton-to-cytoskeleton repulsion interaction (i.e., network swelling) due to electrostatic or entropic forces, one has a ready-made explanation for the memory effect that does not rely on elasticity but rather on the redistribution of the cytoskeleton inside the cell. The decay timescale of this memory is then set by the dissipation timescale of density perturbations which is given by the viscosity divided by the swelling stress (see The Central Role of the Polymerization Signal).

The principal drawback of the cytoskeletal swelling force explanation is, of course, that it lacks direct experimental evidence for its existence. Its principal advantage is that it unifies the issues of memory-like restoring force and protrusive force production in a single solution. On the other hand, the idea of a decaying elastic force has a readily believable origin in the dynamics of cytoskeletal crosslinking. However, the main drawback is that such a mechanism is susceptible to lead to phase separation (see Elastic Force versus Swelling) under stretch condition. Indeed, just as cotton candy fails catastrophically when pulled too quickly, this mechanism may not be able to maintain the cohesion of the cytoskeleton for the high deformation rates ($\leq$1 s) that take place in vivo as neutrophils are sucked into capillaries by the flow of blood.

### Active force generation in neutrophils

#### *Network-network or network-membrane interactions*

Two models were presented in this article: one in which protrusion is caused by a network swelling force and the other in which it is caused by a polymerization force. Of note is that in the second model, some sort of mechanism of force transmission at rest (i.e., that cannot be provided by simple viscosity) is needed. This can be achieved either with elasticity or with swelling, but in the latter case, we have a nonparsimonious solution since swelling is sufficient alone for protrusive force.

As is detailed more thoroughly in the Appendix, these two models can fruitfully be recast into representative examples of two categories of paradigms for cellular forces: network-to-network interactions and network-to-membrane interactions. In the first case, it is an interaction of the cytoskeleton with itself through electrostatic, steric, or molecular motor processes that leads to cellular motion, while in the second case, motion originates from an interaction of the cytoskeleton with the membrane, again through electrostatic, steric, or molecular motor processes. As can be seen from the rather good agreement of our simulations with the experimental data, it is not trivial to discriminate between the two models.

There exists, however, one class of experiments that would make the distinction between the two alternatives. These require the measurement of the motor force (or its proxy, the velocity) against a decreasing load. In the case of network-to-membrane forces, we expect a notable decrease in driving force with decreasing membrane load as in effect, the rug is being pulled from underneath the interaction. For network-to-network forces (swelling) the driving force should remain nearly constant with unloading. This type of experiment could be easily performed by applying varying degrees of suction to a cell crawling in a micropipette and measuring the velocity.

Finally, we would like to point out that from simple thermodynamical arguments, it is expected that in most regimes for which local thermodynamic equilibrium applies, the contribution to the stress energy made by each monomer added to the cytoskeleton should be of order a few $k_BT$ regardless of the precise mechanism of force production. Our calculations show that the maximum total power developed by an activated neutrophil is of order $5 \times 10^{-8}$ erg s$^{-1}$ ($=5 \times 10^{-15}$ J s$^{-1}$). This corresponds to approximately 250,000 monomer additions per s (assuming a contribution of 5 $k_BT$ per monomer). The volume in which such polymerization takes place has to be significant, and this explains why in a more detailed analysis given in the Appendix (Brownian Ratchets), we find that a classical Brownian ratchet relying on the hard-core interaction potential from the dimension of an actin monomer (2.7 nm) is implausible. If a cytoskeleton-membrane interaction is responsible for protrusive forces, its range probably needs to be $>0.1$ $\mu$m.

## CONCLUSION

In this article, we defined three characteristic dynamical parameters of the cortical properties of the neutrophil: baseline tension, slack, and dilation viscosity. These parameters were constrained by data from aspiration experiments, and then shown to yield appropriate results for the pseudopod experiments. Similarly, network polymerization and force production parameters were constrained by the pseudopod experiment and then shown to yield appropriate results for the crawling of neutrophils in a micropipette against counterpressure. While it is not impossible that such consistency is the result of coincidence, it hints at underlying principles that could be elucidated.

By necessity, this work has been a long story to tell. However, the reward of such an effort is that it allows the development of unifying hypotheses that, even though they may sometimes not be valid, can serve as guides in the integration of seemingly disparate data, and in the planning of future experiments. We are well aware that the usual baroqueness and redundancies of real biological systems make it improbable that the simple models that we have offered here

will survive in their current form. But what these models do provide is a convenient starting point for a debate that could eventually lead to a better understanding of macroscopic neutrophil mechanics. Furthermore, although the specialized adaptation of the neutrophil probably has an impact on issues such as the peculiar nature of its surface tension, it is likely that some of the ideas we have explored have applicability to a wide range of amoeboid cells. This will be the topic of future articles.

## APPENDIX

### Another look at the swelling force

The basic idea behind a network swelling stress is that there exists a repulsive force between actin monomers. For free (G-actin) subunits, this has no dynamical consequences as redistribution occurs freely in the cytosol. However, once subunits are sequestered into the cytoskeleton by polymerization, the repulsive force has dynamical consequences because it endows the cytoskeleton with a macroscopic stress. In these conditions, one can intuitively perceive how the energy of the chemical process of polymerization can be transformed into expansion work.

To put these notions on a more formal footing, let us assume that there exists a pairwise repulsive potential force between actin monomers either free or part of a filament. The total force felt by a monomer is therefore:

$$\sum_{\mathrm{i}} \mathbf{F}_{\mathrm{AA^i}} = -\sum_{\mathrm{i}} \frac{\partial \phi_{\mathrm{AA^i}}}{\partial \mathbf{r}_{\mathrm{AA^i}}} \simeq -V_{\mathrm{A}} \nabla \psi^{\mathrm{nn}}, \tag{28}$$

where $\phi$ is the pairwise potential. The second part of the equation assumes that most of the repulsive force derives from fixed monomers sequestered in filaments, such that one can write that the dominant potential contribution is $\psi^{\mathrm{nn}}$, the network-network potential (density) term originally introduced in Eq. 5, and $V_{\mathrm{A}} = (4/3)\pi\delta^3$ ($\delta = 2.7$ nm) is simply the volume of a monomer.

The Gibbs free energy of the polymerization reaction can be written:

$$\Delta G_{\mathrm{pol}} = k_{\mathrm{B}}T \ln \frac{[A^{\mathrm{s}}_{\mathrm{local}}]}{[A^{\mathrm{s}}_{\mathrm{eq}}]}, \tag{29}$$

where $[A^{\mathrm{s}}_{\mathrm{local}}]$ is the true local solvent concentration of free actin at the polymerization site and $[A^{\mathrm{s}}_{\mathrm{eq}}] = k_{\mathrm{off}}/k_{\mathrm{on}}$ is the solvent concentration that leads to no net polymerization.

Let us call $\psi^{\mathrm{sn}}_{\mathrm{A}}$ the work of bringing a monomer from far away to the site of polymerization. We have:

$$\frac{[A^{\mathrm{s}}_{\mathrm{local}}]}{[A^{\mathrm{s}}_{\mathrm{far}}]} = \exp\left(-\frac{\psi^{\mathrm{sn}}_{\mathrm{A}}}{k_{\mathrm{B}}T}\right). \tag{30}$$

Taking Eqs. 29 and 30 together yields:

$$\psi^{\mathrm{sn}}_{\mathrm{A}} = k_{\mathrm{B}}T \ln \frac{[A^{\mathrm{s}}_{\mathrm{far}}]}{[A^{\mathrm{s}}_{\mathrm{eq}}]}. \tag{31}$$

This is the incremental contribution to the network stress $\psi^{\mathrm{nn}}$ obtained by polymerizing one additional monomer at local thermodynamic equilibrium. Thus, by controlling $[A^{\mathrm{s}}_{\mathrm{eq}}]$ through enzymatic activity, the cell has control over swelling stress.

The swelling stress was taken to be linear in the network concentration (Eq. 10):

$$\frac{\partial \psi^{\mathrm{nn}}}{\partial \theta_{\mathrm{n}}} = \psi^{\mathrm{nn}}_0 \tag{32}$$

$$= \frac{\partial \psi^{\mathrm{nn}}}{\partial [A^{\mathrm{n}}]} \frac{1}{V_{\mathrm{A}}} = \psi^{\mathrm{sn}}_{\mathrm{A}} \frac{1}{V_{\mathrm{A}}}, \tag{33}$$

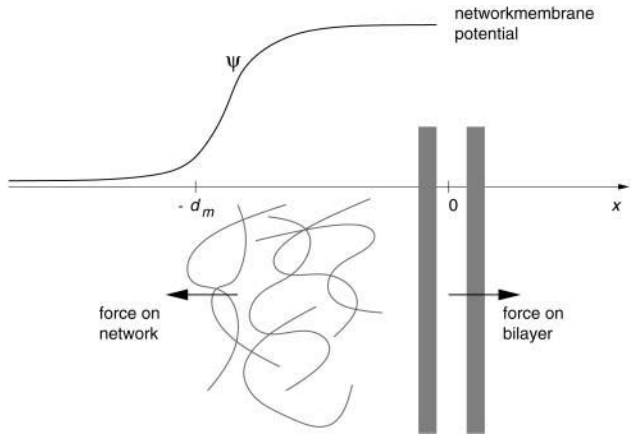


FIGURE 19 General schema of network-to-membrane interactions.

where $[A^{\mathrm{n}}]$ is the network (polymerized) actin concentration. For $\psi^{\mathrm{nn}}_0$ as given in Table 1, we have a stress contribution of 6 $k_{\mathrm{B}}T$ per polymerized monomer, which corresponds to $\ln([A^{\mathrm{s}}_{\mathrm{far}}]/[A^{\mathrm{s}}_{\mathrm{eq}}]) \sim 6$, a plausible value.

It might be argued that in the context of a two-body repulsive force, a swelling stress proportional to $\theta^2$ would have been appropriate. This is correct and would probably work in our calculations; however, we have chosen to keep a linear dependence chiefly as a means to keep an already complex model as simple as possible.

### Another look at the polymerization force

The conceptual and technical details of cytoskeletal membrane interactions turn out to have interesting consequences that we describe here. We begin with a discussion of the effect of disjoining forces at the membrane. We then continue by establishing a connection with the theory of Brownian ratchets. We finally argue that if the picture of membrane cytoskeletal interaction is to explain the processes of neutrophil force generation, this probably involves processes other than short-range Brownian ratchets.

#### *Disjoining forces at the membrane*

Let us consider the interaction potential $\psi^{\mathrm{nM}}(x)$, between membrane and cytoskeleton (see Eq. 11). This potential vanishes everywhere except for a small region of width $d_{\mathrm{M}}$ neighboring the membrane (see Fig. 19). If one then assumes that the cytoskeleton-to-membrane interaction term dominates all others in determining the flow of the network, we have, in the region of width, $d_{\mathrm{M}}$ near the membrane (from Eq. 5 and the conventions of Fig. 19):

$$2\nu \frac{\partial v}{\partial x} = \psi^{\mathrm{nM}}(x). \tag{34}$$

If one integrates this equation from $x = -d_{\mathrm{M}}$ to $x = 0$ (assuming $\nu$ is nearly constant) and writes $\int \psi^{\mathrm{nM}}(x)dx = \psi^{\mathrm{nM}} d_{\mathrm{M}}$, one obtains:

$$v(0) - v(-d_{\mathrm{M}}) = \Delta v = \frac{\psi^{\mathrm{nM}} d_{\mathrm{M}}}{2\nu}. \tag{35}$$

This is the magnitude of the velocity jump leading to retrograde flow of cytoskeleton away from the membrane.

In this article, we have assumed linear constitutive relations such that $\nu = \nu_0\theta$ and $\psi^{\mathrm{nM}} = \psi^{\mathrm{nM}}_0 \tau_{\mathrm{n}} J_{\mathrm{m}} = \psi^{\mathrm{nM}}_0 m\theta$ (where $m$ is the strength of the polymerization signal, $\tau_{\mathrm{n}}$ the network polymerization timescale), so that the velocity jump turns out to be independent of cytoskeletal concentration:

$$\Delta v = \frac{\psi^{\mathrm{nM}}_0 d_{\mathrm{M}}}{2\nu_0} m. \tag{36}$$

For the parameters used in this article (Table 1, $m_{max} \sim 60$), $\Delta v = 6 \times 10^{-5}$ cm s$-$1.

In terms of forward motion at the membrane, the magnitude of the protrusion speed will of course depend on further boundary conditions. In situations of perfect 'bracing' the maximum outward velocity of the membrane is $\Delta v$. However, usual conditions such as the ones considered in this article lead to slippage with backflow of cytoskeleton and the velocity will be less.

### *Brownian ratchets*

Following Peskin et al. (1993), the magnitude of the polymerization strength can be estimated as follows in the Brownian ratchet model. The force due to polymerization of an individual filament is of order $F_M \sim (k_B T/\delta) \ln([A^s]/[A^s_{eq}]$ where $k_B$ is Boltzmann's constant, $T$ is the absolute temperature, and $\delta$ the step size (in this case, the radius of the actin monomer, 3 nm), $[A^s]$ and $[A^s_{eq}]$ are the ambient and equilibrium solvated free monomeric actin concentrations. For first-order kinetics:

$$\frac{[A^s]}{[A^s_{eq}]} = 1 + \frac{1}{\delta}\frac{dL}{dt}\frac{1}{k_{off}}, \tag{37}$$

where $dL/dt$ is the elongation velocity of a polymer, and $k_{off}$ is the reaction off rate.

For situations in which filaments are growing quickly, it is likely that the second term is much larger than 1 since it compares the timescale of net elongation to the timescale of removal of a monomer. Therefore, we have the logarithm of a large number which, as always, can be approximated to 10.

Computing the stress on the membrane due to the polymerization force requires the number of filaments abutting the membrane which we call $F_2$ (cm$^{-2}$) and which is related to the filament volume density $F_3 \sim F_2/l_F$ where $l_F$ is the mean length of a polymer. The pressure exerted on the membrane by the polymerization force is:

$$\psi^{nM} \simeq 10 F_2 \frac{k_B T}{\delta}\varepsilon, \tag{38}$$

where $\varepsilon$ is an efficiency factor of force transduction. This can be rewritten in terms of the network density by using $\theta = F_3[l_F/\delta]/[(4/3)\pi\delta^3]$ :

$$\psi^{nM} = 10 k_B T \frac{\theta}{(4/3)\pi\delta^3}\varepsilon. \tag{39}$$

Numerically ($T \sim 310$ K, $\delta \sim 2.7 \times 10^{-7}$ cm), one obtains $\psi^{nM} = \varepsilon\theta \times 5 \times 10^6$ dyn cm$^{-2}$. As we have described in the previous section, the relevant quantity for the effective load on the membrane is $\psi^{nM} d_M$ where $d_M$ is the range of the cytoskeleton/membrane interaction. For the standard Brownian ratchet with hard-core repulsive potential between the last subunit and the membrane, $d_M \sim \delta$ which leads to $\psi^{nM} d_M \sim \varepsilon\theta \times 1.4$ dyn cm$^{-1}$, more than two orders-of-magnitude lower than what is required by our calculations where $\psi^{nM} d_M = \psi_0^{nM} d_M m\theta \sim \theta \times 7 \times 10^2$ dyn cm$^{-1}$ for $m_{max} \sim 60$. This is grossly insufficient to explain the magnitude of the protrusive forces modeled in this article.

Two comments are in order. The first is that the attentive reader will have noted that by saturating the logarithm, we have broken the direct correlation of force with polymerization rate and transformed it into a potential only dependent on network concentration. (If the argument of the logarithm is small, the reader can check that the force is indeed linear in $\dot{\theta}$.) It so happens that the stimulated polymerization rate used in this article is $J_m = m\theta/\tau_n$ which is linear in the network concentration $\theta$. This is strictly equivalent to postulating a regulated membrane-network repulsion.

The second comment is that the potential range associated with the Brownian ratchet does not have to be $\delta$. Recently Bottino and co-workers (Bottino et al., 2002) have argued that the proper distance scale is the bundling length of filaments sterically interacting with the membrane which is significantly longer than the monomer radius $\delta$. Furthermore, we would argue that other, nonratchet forces (i.e., long-range electrostatic) may generate repulsion between cytoskeleton and membrane and lead to the same result. Finally, it could be that we are grossly underestimating the cytoskeletal concentration right at the membrane and that instead of a volume fraction $\theta_n \sim 10^{-2}$, it is closer to $10^{-1}$, thereby providing a tenfold increase in protrusive force.

This work was supported by National Institutes of Health grant RO1-GM 61806 to M.D.

## REFERENCES

Bathe, M., A. Shirai, C. M. Doerschuk, and R. D. Kamm. 2002. Neutrophil transit times through pulmonary capillaries: the effects of capillary geometry and fMLP stimulation. *Biophys. J.* 83:1917–1933.

Bottino, D., A. Mogilner, T. Roberts, M. Stewart, and G. Oster. 2002. How nematode sperm crawl. *J. Cell Sci.* 115:367–384.

Campbell, M. S., M. A. Lovell, and G. J. Gorbsky. 1995. Stability of nuclear segments in human neutrophils and evidence against a role for microfilaments or microtubules in their genesis during differentiation of HL-60 myelocytes. *J. Leukoc. Biol.* 58:659–666.

Cano, M. L., D. A. Lauffenburger, and S. H. Zigmond. 1991. Kinetic analysis of F-actin depolymerization in polymorphonuclear leukocyte lysates indicates that chemoattractant stimulation increases actin filament number without altering the filament distribution. *J. Cell Biol.* 115:677–687.

Cassimeris, L., H. McNeill, and S. H. Zigmond. 1990. Chemoattractant-stimulated polymorphonuclear leukocytes contain two populations of actin filaments that differ in their spatial distributions and relative stabilities. *J. Cell Biol.* 110:1067–1075.

Dembo, M., and A. K. Harris. 1981. Motion of particles adhering to the leading lamella of crawling cells. *J. Cell Biol.* 91:528–536.

Dembo, M., and F. Harlow. 1986. Cell motion, contractile networks, and the physics of interpenetrating reactive flow. *Biophys. J.* 50:109–121.

Dembo, M., D. C. Torney, K. Saxman, and D. Hammer. 1988. The reaction limited kinetics of membrane to surface adhesion and detachment. *Proc. R. Soc. Lond. B Biol. Sci.* 234:55–83.

Dembo, M. 1989. Mechanics and control of the cytoskeleton in *Amoeba proteus*. *Biophys. J.* 55:1053–1080.

Dembo, M. 1994a. Free boundary and amoeboid motion. *In* Biomechanics of Active Movement and Division of Cells. N. Akkas, editor. NATO Advanced Study Institute Series. Springer-Verlag, Berlin, Germany. pp. 231–283.

Dembo, M. 1994b. Peeling an adherent cell from a surface. *In* Some Mathematical Problems in Biology, Lectures on Mathematics in the Life Sciences, Vol. 25. B. Goldstein and C. Wofsy, editors. American Mathematical Society, Providence, Rhode Island.

Drury, J. L., and M. Dembo. 1999. Hydrodynamics of micropipette aspiration. *Biophys. J.* 76:110–128.

Drury, J. L., and M. Dembo. 2001. Aspiration of human neutrophils: effects of shear thinning and cortical dissipation. *Biophys. J.* 81:3166–3177.

Dunn, G. A. 1980. Mechanisms of fibroblast locomotion. *In* Cell Adhesion and Motility, Third Symposium of the British Society for Cell Biology. A. S. G. Curtis and J. D. Pitts, editors. Cambridge University Press, Cambridge. pp. 409–423.

Evans, E., and A. Yeung. 1989. Apparent viscosity and cortical tension of blood granulocytes determined by micropipet aspiration. *Biophys. J.* 56:151–160.

Evans, E., and W. Rawicz. 1990. Entropy driven tension and bending elasticity in condensed-fluid membranes. *Phys. Rev. Lett.* 64:2094–2097.

Finger, E. B., R. E. Bruehl, D. F. Bainton, and T. A. Springer. 1996. A differential role for cell shape in neutrophil tethering and rolling on endothelial selectins under flow. *J. Immunol.* 157:5085–5096.

Gerbal, F., P. Chaikin, Y. Rabin, and J. Prost. 2000. An elastic analysis of *Listeria monocytogenes* propulsion. *Biophys. J.* 79:2259–2275.

He, X., and M. Dembo. 1997. On the mechanics of the first cleavage division of the sea urchin egg. *Exp. Cell Res.* 233:252–273.

Heinrich, V., and R. E. Waugh. 1996. A piconewton force transducer and its application to measurement of the bending stiffness of phospholipid membranes. *Annals Biomed. Eng.* 24:595–605.

Hill, T. L., and M. W. Kirschner. 1982. Subunit treadmilling of microtubules or actin in the presence of cellular barriers: possible conversion of chemical free energy into mechanical work. *Proc. Natl. Acad. Sci. USA.* 79:490–494.

Hochmuth, R. M., H. P. Ting-Beall, B. B. Beaty, D. Needham, and R. Tran-Son-Tay. 1993. Viscosity of passive human neutrophils undergoing small deformations. *Biophys. J.* 64:1596–1601.

Hochmuth, R. M., J.-Y. Shao, J. Dai, and M. P. Sheetz. 1996. Deformation and flow of membrane into tethers extracted from neuronal growth cones. *Biophys. J.* 70:358–369.

Kan, H.-C., W. Shyy, H. S. Udaykumar, P. Vigneron, and R. Tran-Son-Tay. 1999. Effects of the nucleus on leukocyte recovery. *Ann. Biomed. Eng.* 27:648–655.

Knupp, P., and S. Steinberg. 1994. Fundamentals of Grid Generation. CRC Press, Boca Raton, Florida.

Hochmuth, R. M., and W. D. Marcus. 2002. Membrane tethers formed from blood cells with available area and determination of their adhesion energy. *Biophys. J.* 82:2964–2969.

Kuhlman, P. A., J. Ellis, D. R. Critchley, and C. R. Bagshaw. 1994. The kinetics of the interaction between the actin-binding domain of $\alpha$-actinin and F-actin. *FEBS Lett.* 339:297–301.

Machesky, L. M., E. Reeves, F. Wientjes, F. Mattheyse, A. Grogan, N. F. Totty, A. L. Burlingame, J. J. Hsuan, and A. W. Segal. 1997. Mammalian actin-related protein 2/3 complex localizes to regions of lamellipodial protrusion and is composed of evolutionarily conserved proteins. *Biochem. J.* 328:105–112.

Marsh, D. 1997. Renormalization of the tension and area expansion modulus in fluid membranes. *Biophys. J.* 73:865–869.

Mogilner, A., and G. Oster. 1996. Cell motility driven by actin polymerization. *Biophys. J.* 71:3030–3045.

Needham, D., and R. M. Hochmuth. 1992. A sensitive measure of surface stress in the resting neutrophil. *Biophys. J.* 61:1664–1670.

Peskin, C. S., G. M. Odell, and G. F. Oster. 1993. Cellular motions and thermal fluctuations: the Brownian ratchet. *Biophys. J.* 65:316–324.

Petty, H. R., D. G. Hafeman, and H. M. McConnell. 1981. Disappearance of macrophage surface folds after antibody-dependent phagocytosis. *J. Cell Biol.* 89:223–229.

Rappel, W.-J., P. J. Thomas, H. Levine, and W. F. Loomis. 2002. Establishing direction during chemotaxis in eukaryotic cells. *Biophys. J.* 83:1361–1367.

Rash, P. J., and D. L. Williamson. 1990. On shape-preserving interpolation and semi-Lagrangian transport. *SIAM. J. Statist. Comput.* 11:656–687.

Raucher, D., and M. P. Sheetz. 1999. Characteristics of a membrane reservoir buffering membrane tension. *Biophys. J.* 77:1992–2002.

Rawicz, W., K. C. Olbrich, T. McIntosh, D. Needham, and E. Evans. 2000. Effect of chain length and unsaturation on elasticity of lipid bilayers. *Biophys. J.* 79:328–339.

Ryder, M. I., R. N. Weinreb, and R. Niederman. 1984. The organization of actin filaments in human polymorphonuclear leukocytes. *Anatom. Record.* 209:7–20.

Sanchez, A. J., and L. J. Wangh. 1999. New insights into the mechanisms of nuclear segmentation in human neutrophils. *J. Cell. Biochem.* 73:1–10.

Schmid-Schönbein, G. W., Y. Y. Shih, and S. Chien. 1980. Morphometry of human leukocytes. *Blood.* 56:866–875.

Schmid-Schönbein, G. W., T. Kosawada, R. Skalak, and S. Chien. 1995. Membrane model of endothelial cells and leukocytes. A proposal for the origin of a cortical stress. *Biomech. Eng.* 117:171–178.

Simon, S. I., and G. W. Schmid-Schönbein. 1985. Biophysical aspects of microsphere engulfment by human neutrophils. *Biophys. J.* 53:163–173.

Shao, J.-Y., H. P. Ting-Beall, and R. Hochmuth. 1998. Static and dynamic lengths of neutrophil microvilli. *Proc. Natl. Acad. Sci. USA.* 95:6797–6802.

Sund, S. E., and D. Axelrod. 2000. Actin dynamics at the living cell submembrane imaged by total internal reflection fluorescence photobleaching. *Biophys. J.* 79:1655–1669.

Temam, R. 1979. Navier-Stokes equations theory and numerical analysis. *In* Studies in Mathematics and Its Applications. North-Holland, Amsterdam, The Netherlands.

Ting-Beall, H. P., D. Needham, and R. M. Hochmuth. 1993. Volume and osmotic properties of neutrophils. *Blood.* 81:2774–2780.

Tran-Son-Tay, R., D. Needham, A. Yeung, and R. M. Hochmuth. 1991. Time-dependent recovery of passive neutrophils after large deformation. *Biophys. J.* 60:856–866.

Tsai, M. A., R. S. Frank, and R. E. Waugh. 1993. Passive mechanical behavior of human neutrophils: power-law fluid. *Biophys. J.* 65:2078–2088.

Tsai, M. A., R. S. Frank, and R. E. Waugh. 1994. Passive mechanical behavior of human neutrophils: effect of cytochalasin B. *Biophys. J.* 66: 2166–2172.

Usami, S., S.-L. Wung, B. A. Skierczynski, R. Skalak, and S. Chien. 1992. Locomotion forces generated by a polymorphonuclear leukocyte. *Biophys. J.* 63:1663–1666.

Wachsstock, D. H., W. H. Schwartz, and T. D. Pollard. 1994. Cross-linker dynamics determine the mechanical properties of actin gels. *Biophys. J.* 66:801–809.

Watts, R. G., and T. H. Howard. 1993. Mechanisms for actin reorganization in chemotactic factor-activated polymorphonuclear leukocytes. *Blood.* 81:2750–2757.

Weiner, O. D., G. Servant, M. D. Welch, T. J. Mitchison, J. W. Sedat, and H. R. Bourne. 1999. Spatial control of actin polymerization during neutrophil chemotaxis. *Nat. Cell Biol.* 1:75–81.

Xian, W., J. X. Tang, P. A. Janmey, and W. H. Braunlin. 1999. The polyelectrolyte behavior of actin filaments: a 25Mg NMR study. *Biochemistry.* 38:7219–7226.

Yeung, A., and E. Evans. 1989. Cortical shell-liquid core model for passive flow of liquid-like spherical cells into micropipets. *Biophys. J.* 56:139–149.

Zahalak, G. I., W. B. McConnaughey, and E. L. Elson. 1990. Determination of cellular mechanical properties by cell poking, with an application to leukocytes. *J. Biomech. Eng.* 112:283–294.

Zhelev, D. V., A. M. Alteraifi, and R. M. Hochmuth. 1996. F-actin network formation in tethers and in pseudopods stimulated by chemoattractant. *Cell Motil. Cytoskeleton.* 35:331–344.